



REVIEW ARTICLE

Adaptive optics: principles and applications in ophthalmology

Engin Akyol¹ · Ahmed M. Hagag^{2,3} · Sobha Sivaprasad^{2,3} · Andrew J. Lotery¹

Received: 18 July 2020 / Revised: 19 October 2020 / Accepted: 4 November 2020 / Published online: 30 November 2020

© The Author(s), under exclusive licence to The Royal College of Ophthalmologists 2020

Abstract

This is a comprehensive review of the principles and applications of adaptive optics (AO) in ophthalmology. It has been combined with flood illumination ophthalmoscopy, scanning laser ophthalmoscopy, as well as optical coherence tomography to image photoreceptors, retinal pigment epithelium (RPE), retinal ganglion cells, lamina cribrosa and the retinal vasculature. In this review, we highlight the clinical studies that have utilised AO to understand disease mechanisms. However, there are some limitations to using AO in a clinical setting including the cost of running an AO imaging service, the time needed to scan patients, the lack of normative databases and the very small size of area imaged. However, it is undoubtedly an exceptional research tool that enables visualisation of the retina at a cellular level.

Why do we need adaptive optics?

The visualisation of individual cells had been historically only achievable using histological techniques. Therefore, in vivo cellular imaging of the retina is of great interest to the scientific community. Direct assessment of individual cells in the living retina has the potential to revolutionise our understanding of retinal structure and function in health and disease. The waveguiding property of cone photoreceptors as well as their relatively large diameter in the periphery make them the easiest target for cellular imaging. Towards the end of the last century, in vivo imaging of the cone photoreceptors in normal peripheral retina was achieved using flood illumination (FI) fundus camera [1] and scanning laser ophthalmoscopy (SLO) [2] technologies. In addition, optical coherence tomography (OCT) provided unparalleled sub-cellular axial resolution for the retina [3]. However, the lateral resolution of these systems was limited by wavefront aberrations caused by the optics of the eye.

Optical aberrations are generally classified into chromatic and monochromatic aberrations. Chromatic aberration develops due to the variation in refractive index of eye components for different wavelengths, resulting in inconsistent magnification and positioning of different components of the light at the back of the eye. These aberrations can be overcome using a single wavelength light source. Monochromatic aberrations are wavelength-independent and are commonly divided into low order and high order aberrations. Low order aberrations constitute the greatest proportion and can be corrected using spherical and cylindrical lenses. Although higher order aberrations represent a relatively small proportion of the optical aberrations of the eye, they can significantly reduce lateral resolution and degrade retinal image quality. Adaptive optics (AO) technology was introduced to measure and correct high order aberrations to enhance the resolution and image quality of the existing imaging modalities.

Brief history of adaptive optics

The history of AO started in astronomy. Horace Babcock originally proposed the use of AO to correct the dynamic wave-front error that atmospheric turbulence causes in ground-based telescopes [4]. Since then it has been possible to measure the total optical aberrations of the human eye using a Shack-Hartmann wavefront sensor (SHWS), an essential piece of innovation in the development of AO. Moreover, Dreher and his group then introduced a deformable mirror another an essential component of AO

These authors contributed equally: Engin Akyol, Ahmed M. Hagag

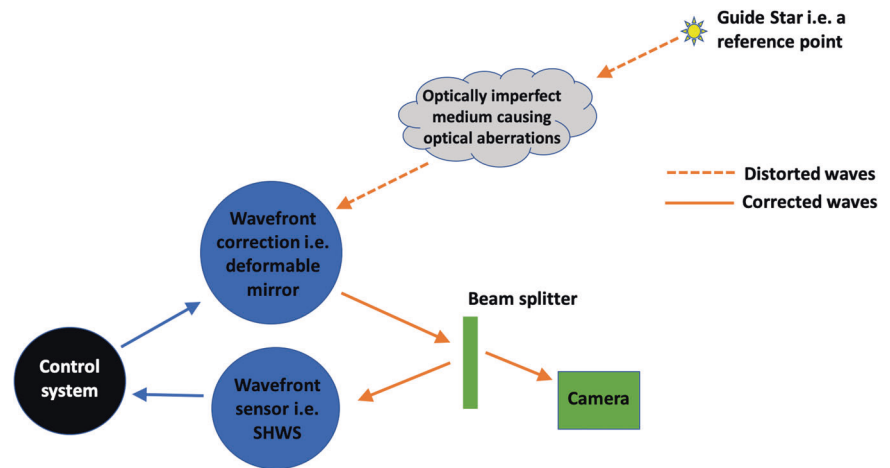
✉ Andrew J. Lotery
a.j.lotery@soton.ac.uk

¹ Faculty of Medicine, University of Southampton, Southampton SO17 1BJ, UK

² NIHR Moorfields Biomedical Research Centre, Moorfields Eye Hospital NHS Foundation Trust, London EC1V 2PD, UK

³ UCL Institute of Ophthalmology, London EC1V 9EL, UK

Fig. 1 Image showing how the different components of an adaptive optic system come together to overcome the optical aberrations of the eye.



scanners [5] to correct the measured aberrations. AO is capable of correcting the total wave aberration of the eye. The first use of AO in ophthalmic practice was reported in 1997 [6]. Liang et al. was the first to combine a SHWS with a deformable mirror to correct aberrations and obtain high-quality images of the retina.

The first clinical use of AO was in 2000 to assess cone-rod dystrophy [7]. Since then multiple studies have been carried out in assessing cones, rods, retinal vessels and other retinal structures such as drusen, microaneurysms, haemorrhage, etc. AO can complement other forms of retinal imaging such as spectral-domain OCT, fundus autofluorescence (FAF), fundus fluorescein angiography (FFA), indocyanine green angiography (ICG) etc in helping understand retinal disease.

Principles of Adaptive Optics

In addition to ocular aberrations, high-resolution imaging of the retina also faces the challenge of limited reflectance of the retina, in particular the retinal pigment epithelium (RPE), photoreceptor inner segments and retinal ganglion cells (RGC) [8]. The principles of adaptive optics were invented by astrophysicists to help improve the quality of images of distant stars obtained by telescopes. The issue, when analyzing distant objects with a telescope, was the lack of clarity of these objects due to the blur-inducing optical aberrations caused by turbulence within the earth's atmosphere. The principles used in telescopes have since been translated into ophthalmic practice to view the retina at a cellular level. The human eye is not an optically perfect system and irregularities within the cornea, lens and vitreous makes viewing the retina difficult. These distortions limit image quality and AO uses four components that work together to remove these distortions—wavefront sensor, wavefront correction, control system and artificial guide star

(Fig. 1). The eyes best optical performance occurs with a pupil ~3 mm in diameter. However, for retinal examination, the pupils will need to be dilated to about 8 mm when significantly more aberrations occur. The development of AO allows the possibility of projecting aberration-free images on the retina with large pupil diameters.

Resolution

AO has the ability to resolve cones and rods in the retina [9] as well as the finest retinal vasculature. AO can resolve to 2 μm but there is substantial difference in resolving rods over cones which is most likely down to the smaller sizes of rods. The resolution of an imaging system is determined by the following formula:

$$r = 0.61\lambda/NA$$

(r is the resolution, λ the imaging wavelength, and NA is the numerical aperture).

In theory the expected limit of achievable lateral resolution is about 2 μm , this limit is not reached because the eye is not diffraction-limited even for monochromatic light.

Wavefront sensor and wavefront correction

The principle behind AO imaging is to identify the optical aberrations of the eye and to then correct for these imperfections (Fig. 1). AO systems require three different components: a wavefront sensing component, a wavefront correcting component and a controller. The aim of the controller is to link the first two components.

Wavefront sensing requires a beacon of light to act as a guide star i.e., a reference point from which the measurements can be made. A variety of different wave front sensors exist but the most commonly used is the SHWS. We can measure the optical aberrations of an eye using the SHWS [10] and it is this that has made AO imaging possible. Other types of wavefront sensors exist e.g., the

pyramid sensor [11]. The SHWS is made of lenslets placed at the focal distance, the aim of which is for each lenslet to focus collimated light on to an area detector i.e., a charge coupled device or a complementary metal–oxide–semiconductor. A planar wave that is incident on the SHWS is used as the reference to produce spots on the camera. Any deviations from this reference wavefront will produce displacements of each spot that can be represented in the cartesian coordinate system of the camera.

The other essential part of the AO imaging devices is the wavefront correction. The most commonly used is the deformable mirror as this can be used to counter the aberrations measured by the SHWS. Other types of wavefront correction devices include a liquid spatial light modulator [12] or segmented mirrors [13, 14]. Some systems use two deformable mirrors to compensate for a larger variety of aberrations. The way in which a deformable mirror works is by changing the surface shape under experimental control to compensate for the eye's optical aberration. The limited range of shapes of deformable mirrors initially limited the amount of aberrations that could be corrected [5], however, this is now much improved.

Types of adaptive optics

AO technology is basically a technique to overcome optical aberrations. Thus, in theory, it can be incorporated with almost any ophthalmic imaging modality to increase resolution to cellular/subcellular level. To date, AO has been combined with flood illumination ophthalmoscopy (AO-FIO), scanning laser ophthalmoscopy (AO-SLO), as well as optical coherence tomography (AO-OCT).

Adaptive optics flood illumination ophthalmoscopy

One of the earliest approaches to utilise AO in ophthalmology was through merging it with a fundus camera [6]. In an AO-FIO system, the whole region of interest is illuminated simultaneously, and the entire frame is captured concurrently from backscattered light. Therefore, images can be acquired in a relatively short time, minimising the effect of eye movement. However, this approach limits the axial resolution of images. In addition, defocused scattered light from the retina and choroid can still be included in the image resulting in reduced contrast as compared to SLO-based systems [15]. The rtx1 (Imagine Eyes, Orsay, France) is an example of a compact FIO-based commercially available AO system [16]. The system has been used for investigating parafoveal cone photoreceptors and retinal vasculature in normal subjects as well as several eye diseases (Figs. 2–5) [17–19].

Adaptive optics scanning laser ophthalmoscopy

In contrast with FIO systems, SLO uses a focused single-spot light beam to raster scan the retina [20]. Backscattered light is refocused onto a confocal aperture to eliminate the effect of stray defocused light, therefore enhancing contrast and axial resolution [9]. Confocal detection allows for imaging the waveguiding photoreceptor outer segments (OS) and the highly-reflective nerve fibres, lamina cribrosa and blood vessels [21]. More recently, non-confocal light detection modes have been proposed to benefit from a multiply scattered light surrounding central focused signal [22]. “Offset aperture” imaging can enhance the visualisation structures that scatter light in one direction such as retinal ganglion cells [23]. “Dark-field” imaging involves blocking the confocal signal and detecting the whole surrounding annular signal, and has been used to visualise the RPE pattern [24]. In “split-detection” imaging mode, the annular signal can be divided into two detectors to reveal photoreceptor inner segments [25].

Adaptive optics optical coherence tomography

Spectral-domain OCT has the ability to provide cross-sectional images with unparalleled axial resolution. However, monochromatic aberrations of the eye limit its lateral resolution to about 15–20 μm [26]. In addition, the interferometric nature of OCT results in introducing granular speckle noise that can obscure detailed microscopic features. Incorporating the AO technology into OCT can significantly improve lateral resolution and reduce speckle size [27, 28]. Thus, facilitating high-resolution three-dimensional imaging of retinal cells/structures and even biological processes [29].

Adaptive optics-based metrics

Photoreceptors

Cone photoreceptors were one of the earliest cells to be visualised and quantified in the retina using AO. Cone photoreceptors are normally arranged in an imperfect hexagonal lattice pattern [30]. The identification of cones is most commonly performed using semi-automated approaches, in which the centre of cone photoreceptors is initially detected automatically, and then reviewed by an experienced human grader for manual corrections (Fig. 2) [31]. Although highly reliable, this approach can be intensively laborious and time consuming. Thus, new tools are actively being developed to improve the performance of automated detection of photoreceptors [32].

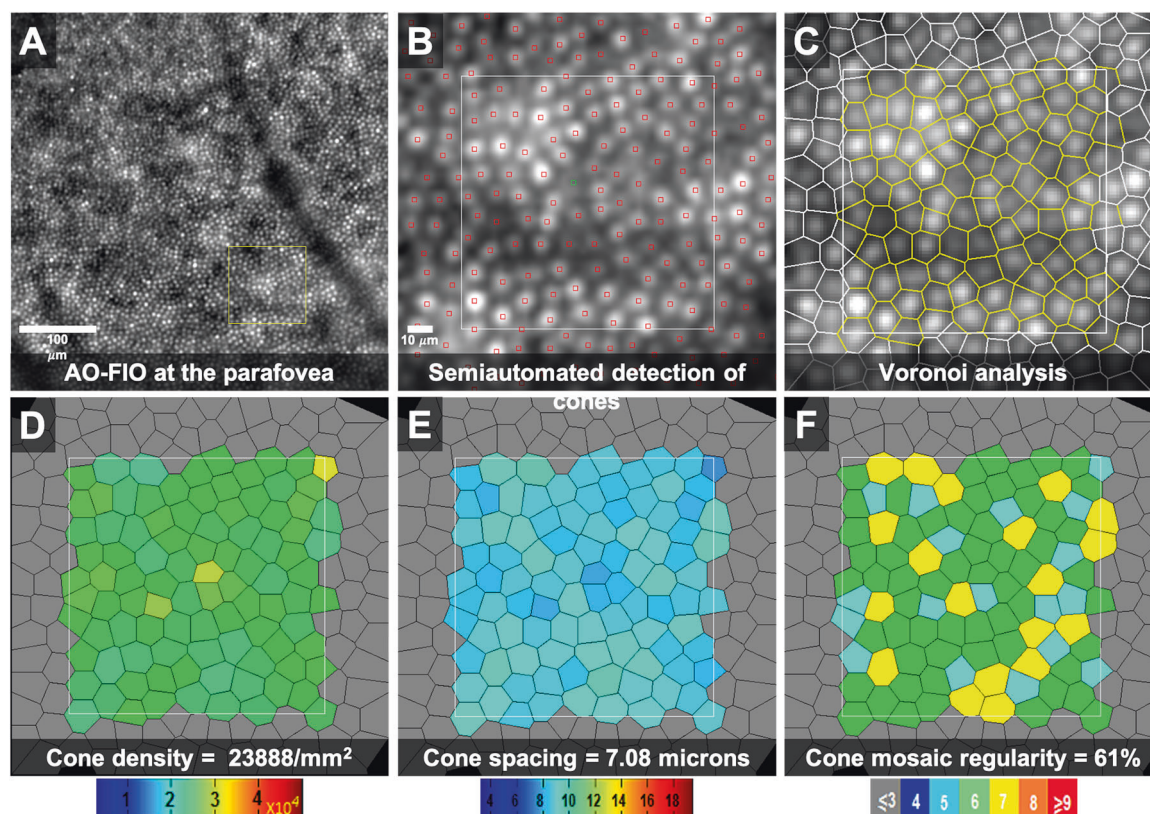


Fig. 2 Adaptive optics flood illumination ophthalmoscopy (AO-FIO, rx1, Imagine Eyes) imaging of the cone photoreceptor mosaic in the right eye of a 36-year-old female healthy volunteer. Quantitative analyses were performed on the AODetect software (Imagine Eyes). **a** 0.5×0.5 mm image captured at a location 2 degrees temporal to the centre of the fovea. The area inside the yellow square

was enlarged in **b–f** to extract measurements. **b** The centre of cones was identified automatically (small red squares) and then validated/corrected by a human grader (green square). Voronoi analysis of the cone mosaic (**c**) was performed to calculate and construct colour-coded maps of cone density, spacing and regularity (**d–f**, respectively).

After the identification of cells, several metrics can be automatically measured (Fig. 2) [33]. Cone density and spacing are the most commonly utilised biomarkers [34]. Photoreceptor density is calculated by simply dividing the number of cones within a region by the area. For spacing parameters, distances between adjacent cells (neighbours) are used to perform Voronoi mapping of the cone mosaic (Fig. 2) [35]. Inter cell distance is defined as the mean distance between each cone photoreceptor and its neighbours. Nearest and farthest neighbour distances has been also described to define the minimum and maximum space between each cone and its neighbours in the submosaic [33]. Voronoi analysis can also provide information on the regularity of the cone mosaic [36]. Prevalence of cells with exactly six neighbouring cells can indicate the degree of hexagonality, hence regularity, in the cone mosaic (Fig. 2). The reliability of cone density and distancing measurement was found to be dependent on sampling window size and analysis methodology. Intrasession repeatability can be as good as 2.7% with a larger sampling window, image alignment and semi-automated cone identification methods [34].

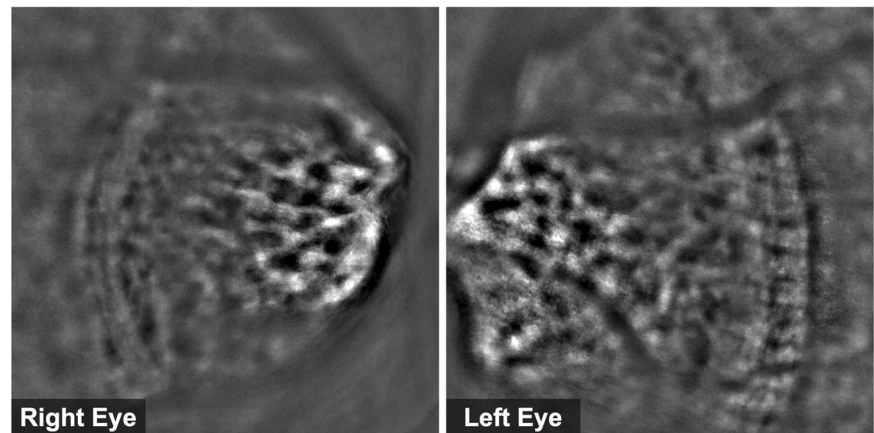
More recently, photoreceptor size measurements were proposed to describe cell degenerative processes. Split-detection AO-SLO was used to visualise and measure the diameter of photoreceptor inner segments [37]. In addition, the high axial resolution provided by AO-OCT allowed for sensitive measurement of the outer segment length [38]. However, the significance and applicability of these size metrics still needs to be studied.

Cone photoreceptor reflectivity has been also measured and used as a metric [39]. Dysflective cones can be detected in AO-FIO, AO-SLO and AO-OCT images, representing non-waveguiding cones outer segments [33, 40]. Although cone reflectance was proposed to correlate with function, several studies concluded that the relationship between them is not straightforward [41]. This is discussed in detail in “How does adaptive optics relate to visual function?” section of this review.

Retinal pigment epithelium

Fluorescence and dark field AO-SLO techniques have been used for RPE imaging [24, 42]. Direct visualisation of RPE

Fig. 3 Lamina cribrosa from the right and left eyes of a 35-year-old healthy female. Images were taken using a commercial adaptive optics flood illumination camera (rtx1, Imagine Eyes).



in normal retina using confocal AO-SLO has been challenging. However, RPE was successfully imaged in cases with photoreceptor loss or subretinal detachment [43]. Thus, the embedment of photoreceptor outer segments into RPE has been linked to the difficulty of RPE visualisation. The previously described photoreceptor cell density and spacing techniques were similarly utilised for RPE quantification [44]. Multimodal AO imaging allowed for simultaneous measurement of RPE and photoreceptor densities to calculate the RPE-to-photoreceptors ratio in healthy and diseased retina [45]. In addition, reflectance-based analysis of AO-OCT images of the photoreceptor-RPE complex has been described to characterise organelle motility and light scatter pattern [46]. Liu et al. performed repeated measurement of organelle motility at the same retinal location in 1 subject to assess variability [46]. A 3% difference was calculated between repeated measurements [46]. However, extensive reliability investigations still need to be performed on large cohorts to validate the potential of RPE-related metrics.

Retinal ganglion cells

The in-vivo visualisation of RGCs has been difficult due to their transparency and dense three-dimensional geometry. Multi-offset AO-SLO imaging was used to produce 2D images of a monolayer of RGCs at areas with limited overlying NFL [47]. Cell somas were segmented manually to measure the distribution of cell diameter and area [47]. Liu et al. used 3D AO-OCT volumes to investigate the tomography of the inner retina including GCL [23]. However, GCs and displaced amacrine cells could not be differentiated within the GCL. Soma diameter and stack thickness at different retinal locations were measured based on the *en face* reflectance projection of a 3-pixel thick slabs around cell centres. GCL soma reflectivity was also measured at the centre of the cells [23]. GC counts and densities were measured at different retinal eccentricities after subtracting amacrine cell number estimates from the literature.

AO-OCT was also able to distinguish parasol and midget GC subtypes based on cell size, density and reflectivity [23]. The GC-to-cone ratio was also calculated across different locations. The reliability of these metrics still needs to be studied.

Lamina cribrosa

The lamina cribrosa has always been an area of interest for pathophysiological investigations in glaucoma. Confocal AO-SLO and AO-FIO imaging allowed for high resolution 2D visualisation of the lamina cribrosa (Fig. 3) and quantitative analysis of pore geometry [48]. Several groups utilised manual delineation of pore boundaries in AO-SLO images to calculate pore number, density and area [48]. The pore ovality index was also measured as the ratio between major and minor axes of the best-fitted ellipse. Nearest neighbour distance of each pore was also determined after the identification of pore centroid location [48]. Distance and area measurements can be corrected for individual's axial length using Littmann's method [49]. Ivers et al. acquired repeated measurements to assess intrasession and intersession variability in normal eyes [48]. Pore geometry metrics had an excellent repeatability of <1%. However, they reported larger intersession variability, ranging from 4% for distance measurements to around 8% for pore elongation and area parameters [48]. More recently, with the development of AO-OCT technology, three-dimensional parameters were introduced to characterize the microstructure of the lamina cribrosa [50]. Semi-automated methods were developed for pore and beam segmentation. Connective tissue volume fraction was defined as the percentage volume of voxels occupied by beams within the analysed lamina cribrosa [50]. Local thickness was measured at each voxel within a region of interest (pore or beam) as the diameter of the largest fitting sphere inside the region. Pore diameter and beam thickness were calculated by averaging the assigned local thickness

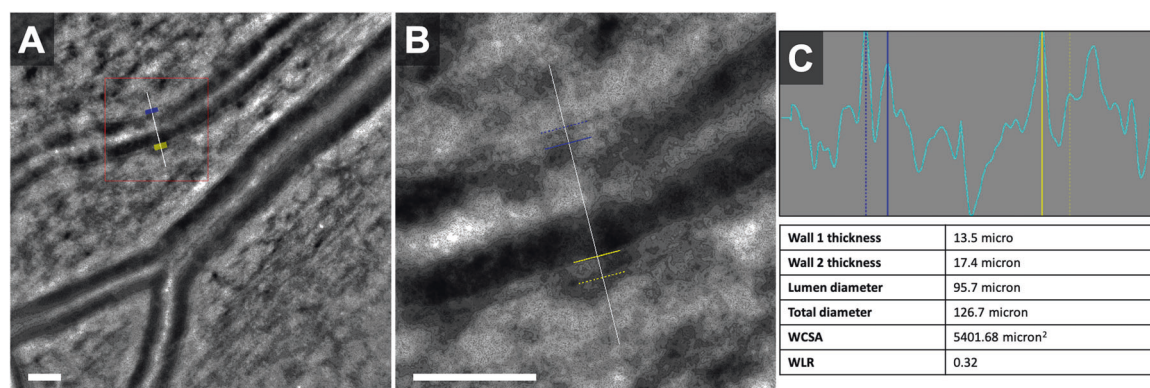


Fig. 4 Imaging retinal vessels using adaptive optics flood illumination ophthalmoscopy. Images were taken from the right eye of a 36-year-old healthy female. **a** The structure of retinal arteriole and venules can be visualised. **b** Enlarged image of the arteriole, corresponding to the red square in **a**. **c** Gradient profile orthogonal to the blood vessel (corresponds to the white line in **b**). Edges of the vessel

wall (blue and yellow lines) were automatically identified from the orthogonal gradient profile. Wall thickness, lumen diameter, total vessel diameter, cross-sectional area of vessel wall (WCSA), and wall-to-lumen ratio (WLR) were calculated for the vessel of interest. The white scale bars in **a** and **b** represent 100 μm .

values of the corresponding voxels [50]. A reliability study revealed high repeatability of 3D AO-OCT parameters in normal and glaucomatous eyes. Nadler et al. reported a variability of $\leq 4.7\%$ in the measurement pore area and diameter, beam thickness and connective tissue volume fraction using their automated segmentation [50]. However, they reported poor repeatability in measuring lamina volume due to the unreliable identification of external lamina cribrosa boundary [50]. More studies are still needed to investigate intersession reproducibility of these parameters.

Retinal vasculature

Several AO systems and imaging modalities allowed for exquisite visualisation of blood vessel wall, lumen and blood cells, enabling the assessment of vascular morphology and perfusion [51]. Arteriolar wall thickness and lumen diameter can be measured reliably from AO images (Fig. 4) [52]. Meixner et al. reported intra-observer measurement variability of 6 and 2% for vessel wall thickness and total vessel diameter, respectively [18]. Wall-to-lumen ratio (WLR) is a commonly used metric to evaluate structural changes in retinal arterioles [18, 53]. Lumen diameter and total vessel diameter were found to exhibit a strong linear correlation across different vessel sizes in normal subjects [54]. Thus, WLR can be highly predictable for a given vessel size. Deviations from this relationship can be used as a disease biomarker [54]. The cross-sectional area of vascular wall (WCSA) can be also measured based on vessels and lumen diameters (Fig. 4) [18]. Retinal vessel branching has been also investigated in health and disease [55]. Arteries and veins were imaged at bifurcation sites across a wide range of vessel sizes. Bifurcation angle and the diameter of parent and daughter

vessels can be measured from structural images and perfusion maps [55].

High-resolution images of retinal capillary networks can be also generated by acquiring overlapping AO images and using motion inside blood vessels as a contrast to construct parafoveal perfusion maps non-invasively, a similar concept to the OCT angiography technology [56]. Several metrics have been introduced to characterize retinal microvascular changes. Foveal avascular zone (FAZ) area has been segmented and measured using manual or semiautomated approaches [56, 57]. The effective diameter of the FAZ was also calculated as the diameter of the circle with equal area [58]. The boundary of the FAZ was used to calculate an acircularity index, defined as the ratio between perimeter of the FAZ and the circumference of the circle with equal area [58]. Capillaries can also be identified within a region of interest to measure the total length of extracted capillaries. Capillary density has been also calculated as a ratio between total capillary length and the total area of the region of interest. A tortuosity metric has also been described based on vessels curvature [58]. Curvature was calculated using a sliding least-squares polynomial fitting approach [53].

Retinal blood flow

Individual leukocytes can be directly visualised in confocal AO-SLO videos. Due to the relatively low absorption and scattering of leukocytes as compared to other blood components, they allow more light to reach photoreceptors and then reflect back [59]. Thus, they appear as hyperreflective particles moving inside darker vessels. Observing leukocyte movement within capillaries can be potentially used for in vivo investigation of leukocyte-endothelial interactions in humans [59]. Leukocyte velocity can be also calculated after measuring the distance travelled by the cell in

successive 2D frames [60]. Axial length should always be taken into account when measuring retinal distances to overcome the effect of optical magnification [49]. However, Martin et al. observed significant variability in velocity measurements between repeated sessions [61]. Pulsatility of leukocytes can be determined by analysing the association between the measured velocity and cardiac cycle [62]. Each cardiac cycle was tracked simultaneously during retinal imaging, and then divided into five equal segments. Leukocyte velocity measurements were computed from video frames and a mean velocity was assigned to each cardiac cycle segment. The difference in mean velocity between highest and lowest segments ($V_{\max} - V_{\min}$) and the average of all measured leukocyte velocities (V_{mean}) were calculated. A pulsatility index (P) was then defined as $P = (V_{\max} - V_{\min})/V_{\text{mean}}$ [62]. Spatiotemporal plots of a selected vessel have also been generated from AO-SLO videos by plotting the intensity along the centre of the vessel of interest against frame number [63]. Objects within vessels can be then traced from the plots to extract hemodynamic information, including flow direction, speed, pulsatility, as well cell distribution and trafficking across different vessels [63].

Spatiotemporal plots (XT images) can be also constructed from repeated 1D line scans across the vessel of interest to trace the movement of blood cells [64]. Moving erythrocytes appear as diagonal bright lines within the imaged vessels. Velocity of RBC movement can be calculated from the slope of these diagonal streaks [65]. Palochak et al. confirmed the precision of this method by measuring blood flow in parent and daughter vessels at a bifurcation in a healthy control and two diabetic patients [66]. Further studies are still needed to assess the reliability of AO-derived blood flow measurements.

How does adaptive optics relate to visual function?

The ability of AO to resolve individual photoreceptors has enabled cell-targeted functional testing [67]. Spatiotemporal variation in photoreceptor reflectance is a prominent feature in AO images [8, 39]. Photopigment bleaching can change cone photoreceptor reflectivity. By employing selective bleaching and retinal densitometry techniques, it is possible to characterize the arrangement of the trichromatic cone mosaic at the cellular level [68]. In addition, several other factors have been linked to changes in cone reflectivity, including OS length and integrity, phototransduction, visual stimulation and direction of illumination [69, 70]. The relationship between photoreceptor reflectivity and function is not fully understood. Areas with decreased cone reflectance are reported to exhibit no functionality in several retinal diseases including age-related macular degeneration

(AMD) [71] and achromatopsia [22]. In contrast, other investigators reported residual sensitivity in those areas in AMD [72] and macular telangiectasia [73]. In addition, in normal eyes, no correlation was observed between cone reflectivity and sensitivity [41]. Temporal changes in the reflectivity of rod photoreceptors has also been detected in healthy and diseased retinas [8].

The AO-OCT has been also used to characterize physiological changes in photoreceptors. Temporal changes in the reflectivity of cone OS tips as well as the decrease in OS length have been attributed to disc shedding and phagocytosis by RPE [74]. AO can also be used to present diffraction limited tiny visual stimuli to target the centre of a photoreceptor, inter-cell space or a small group of photoreceptors [75]. This can be achieved by modulating the imaging light or using a second channel to provide visual stimuli [76]. Grieve and Roorda used AO-SLO to study the single cone response to checker board pattern visual stimuli [69]. They reported a variable response in cones, with some cones showing increased reflectance while others might show a decrease in reflectivity. Similar AO-based techniques are being extensively used for detailed investigation of visual processing in the human retina [77].

Vascular autoregulatory processes have also been investigated by AO technology. AO-SLO and AO-FIO reveal a focal increase in retinal blood velocity and/or vessel diameter in response to local visual stimulation [78]. Thus demonstrating the neurovascular coupling previously described in neural tissue, including the retina [79]. Furthermore, AO perfusion maps can reveal autoregulatory microvascular dilation or constriction in response to hypercapnea and hyperoxia, respectively [80]. Similar responses have been previously described using other imaging modalities including OCT angiography [81].

Table 1 summarises quantitative metrics derived from AO images and their definition.

Clinical applications of AO

Healthy eyes

It is essential to analyse healthy eyes using AO as the results can be used to help develop normative databases. This can then be used in clinical practice when assessing patients i.e., identifying deviations from normal. At present there needs to be an expansion in the volume of healthy eyes imaged with AO. Below we will discuss some of the relevant studies looking at healthy eyes using AO.

Firstly, AO-SLO has been used to measure the variation of cone packing density across the retina in healthy subjects of different ages [82]. This group tested ten younger subjects (age range, 22–35 years) and ten older subjects (age

Table 1 A summary of adaptive optics-based metrics and their definitions.

Adaptive optics metric	Definition
Photoreceptors and retinal pigment epithelium (RPE)	
Density	Number of cones per unit area (Fig. 2)
Inter-cell distance	Mean distance between each photoreceptor and its neighbours (Fig. 2)
Nearest and farthest neighbour distance	Minimum and maximum space between each photoreceptor and its neighbours in the submosaic.
Cone hexagonality	Prevalence of cone photoreceptors with exactly 6 neighbouring cells (Fig. 2)
RPE-to-photoreceptor ratio	Ratio between the numbers of RPE cells and photoreceptors within an area of interest
Reflectance	The average intensity of pixels corresponding to photoreceptors
Retinal ganglion cells (RGC)	
Cell soma area	The total area of pixels within the manually segmented boundary of a cell soma from a 2D image
Cell soma diameter	The diameter of a circle with an equivalent area
Stack thickness	The number of RGC soma arranged in a vertical stack
Cell counts and density	The number of soma measured from the <i>en face</i> image after subtracting the amacrine population values from the literature
Ganglion cell-to-cone ratio	Ratio between the numbers of ganglion cells and cone photoreceptors at specific location
Lamina Cribrosa	
Pore number, density and area	Pore metrics can be calculated after manual delineation of pore boundary
Pore ovality index	Ratio between major and minor axes of the best fitted ellipse to each pore
Nearest neighbour distance	The minimum distance between the centroid of a given pore and that of its neighbours
Connective tissue volume Fraction	Percentage volume of voxels occupied by beams within an area of interest
Pore diameter and beam thickness	The average local thickness of the corresponding voxels. Local thickness at each voxel within a region (pore or beam) is measured as the diameter of the largest fitting sphere inside the region.
Retinal Vasculature	
Wall thickness and lumen diameter	Vessel wall edges can be identified from the intensity gradient profile at a line orthogonal to the direction of blood flow. Wall thickness and lumen diameter can then be measured (Fig. 4).
Wall-to-lumen ratio (WLR)	Ratio between vessel wall thickness and lumen diameter (Fig. 4)
Wall cross-sectional area (WCSA)	$(\text{Wall thickness 1} + \text{wall thickness 2} + \text{lumen diameter})^2 - (\text{lumen diameter})^2$ (Fig. 4)
Bifurcation angle	The angle between the two daughter vessels of a branching parent vessel
Foveal avascular zone (FAZ) area	The area of FAZ after manual or automated segmentation of FAZ boundary
Effective diameter of FAZ	The diameter of a circle with equal area
FAZ acircularity index	The ratio between perimeter of the FAZ and the circumference of the circle with equal area
Total capillary length	Total length of extracted capillaries within a region of interest
Capillary density	The ratio between total capillary length and the total area of region of interest
Tortuosity	The ratio between total squared curvature of the vessel and the length of the vessel
Blood cells	
Velocity	Distance travelled per unit time
Pulsatility index	The ratio between the difference between maximum and minimum blood cell velocity and the mean blood velocity ($P = (V_{\max} - V_{\min})/V_{\text{mean}}$)

All distance and area measurements need to be adjusted for axial length.

range, 50–65 years). They showed cone packing density was higher closer to the fovea and decreased with increasing retinal eccentricity. They found that older subjects had ~75% of the cone density at ~0.6° from the fovea compared to the younger group. This study demonstrates that normal values may be different for different age groups.

In a separate but similar study the cone packing density was again measured using an AO-SLO [83]. Cone density was analysed as a function of retinal eccentricity, refractive error, axial length, age, gender, race/ethnicity and ocular

dominance. Cone packing density was measured at three different retinal eccentricities 0.5, 1.0 and 1.5 mm from the foveal centre. Cone density decreased from 32,200 to 11,600 cells/mm² with retinal eccentricity. It demonstrated cone packing density decreases as a function of retinal eccentricity and axial length. However, gender, ocular dominance and race/ethnicity were not important determinants of cone density. Again, the data for different factors e.g., race and gender need to be well established before AO can be applied to clinical use.

More recently a group in France used an AO retinal camera (RTX-1[®] Imagine Eyes) [19] to assess healthy eyes belonging to patients of various ages. They measured cone density together with cone spacing and cone mosaic packing in the nasal and temporal area 450 μm from the fovea. Their results showed that perifoveal cone density significantly decreased with age whereas cone spacing increased with age. In this study age and axial length were shown to be related to a cone density decrease, while choroidal and retinal thicknesses did not affect cone metrics in healthy subjects. The recurring theme here is that age and axial length are important factors when evaluating cone density.

Finally, another group again use the AO flood-illumination retinal camera (rtx1) to measure cone density in the eyes of healthy individuals. This study included 33 patients and the median cone density was 19,269 cones/mm as measured 3 degrees from the fovea [84].

Data from patients with so-called normal eyes is essential to help build the data of expected AO parametric values. A uniform way of measuring photoreceptor density and spacing should be established in order for all researchers/clinicians to carry out the above assessments in a standardised way. Clinicians need to be taught how to interpret these images and be given information on what AO images/results mean for their patients.

Diabetic retinopathy (DR)

AO has been used to evaluate parafoveal cone density in patients with Type 1 diabetes mellitus [85]. Of the patients in the study, five had a diagnosis of no diabetic retinopathy and six had mild non-proliferative diabetic retinopathy. The results showed that cone density was 10% lower in the study than in the control group at each retinal eccentricity along the horizontal and vertical meridians. This study suggests AO can identify early retinal changes of diabetes not detectable by other forms of imaging or by clinical examination (Fig. 5).

Furthermore, AO has been used in diabetics to look at the FAZ, microaneurysms and drop out of capillaries at the edge of the FAZ [86]. AO-SLO videos of the parafoveal region from patients with type 2 diabetes and no retinopathy and from control subjects were assessed. An increased average tortuosity of arteriovenous channels in patients with type 2 diabetes were seen even though there were no signs of DR in these eyes. This again highlights the clinical application of AO in detecting early changes in eyes which appear to be not clinically affected by diabetes.

A study presented at the Association for Research in Vision and Ophthalmology meeting in 2012 showed the cone photoreceptor mosaic pattern can be disrupted in diabetic retinopathy in patients with type 1 diabetes using AO-SLO

[87]. Interestingly, alterations in photoreceptor density and arrangement are most evident in the superotemporal quadrant in eyes with diabetic macular oedema [87].

In contrast, another study found that parafoveal cone photoreceptor density in type 1 diabetics was not reduced and was found to be similar to controls [88]. Given this difference in findings between the above studies further studies looking at cone densities are crucial.

There is no doubt that AO is now able to pick up finer changes in blood vessels in patients with diabetic retinopathy [89] helping us better understand the underlying pathology of diabetic retinopathy. A study of retinal capillary lumen calibre in patients with type 1 diabetes was analysed. It showed that average capillary lumen calibre was significantly narrower in eyes with non-proliferative diabetic retinopathy compared with control eyes. These vascular changes are an indication of early diabetes-induced damage. Clinically if these changes could predict which patients will progress, early intervention could be applied to reduce the progression.

AO-SLO is able to identify and visualise individual microaneurysms [90] and some of these microaneurysms have quite different appearances. AO-SLO offset pinhole motion contrast (utilises an off-centre pinhole with no need for an external contrast agent) can provide perfusion maps comparable to those obtained with AO-SLO FA, while AO-SLO OP reflectance images provide additional information such as vessel wall fine structure.

AO is useful in gaining a better mechanistic understanding of DR. It can image microaneurysms, blood vessels and cone cells. These are all targets that are damaged in DR.

Central serous chorioretinopathy (CSCR)

AO has been used to assess central serous chorioretinopathy. A case presentation revealed that AO optics demonstrated lower density, spacing and changes in the photoreceptor mosaic pattern in the left eye which had recovered from CSCR than in the right eye, suggesting that CSCR may cause damage to cones after clinical recovery [91]. A more comprehensive comparison with AO-SLO in 45 eyes with resolved CSCR and 20 normal eyes demonstrated abnormal cone mosaic patterns and reduced cone densities in eyes with resolved CSCR, and these abnormalities were associated with VA loss [92]. In a separate study, patients who had CSCR were followed up with AO-SLO for 12 months once the CSCR had resolved. The results revealed a gradual increase in macular cone densities over a 12-month period in patients with resolved CSCR [93]. These studies demonstrate another potential role for AO in patients with CSCR i.e., to monitor patients post resolution of CSCR.

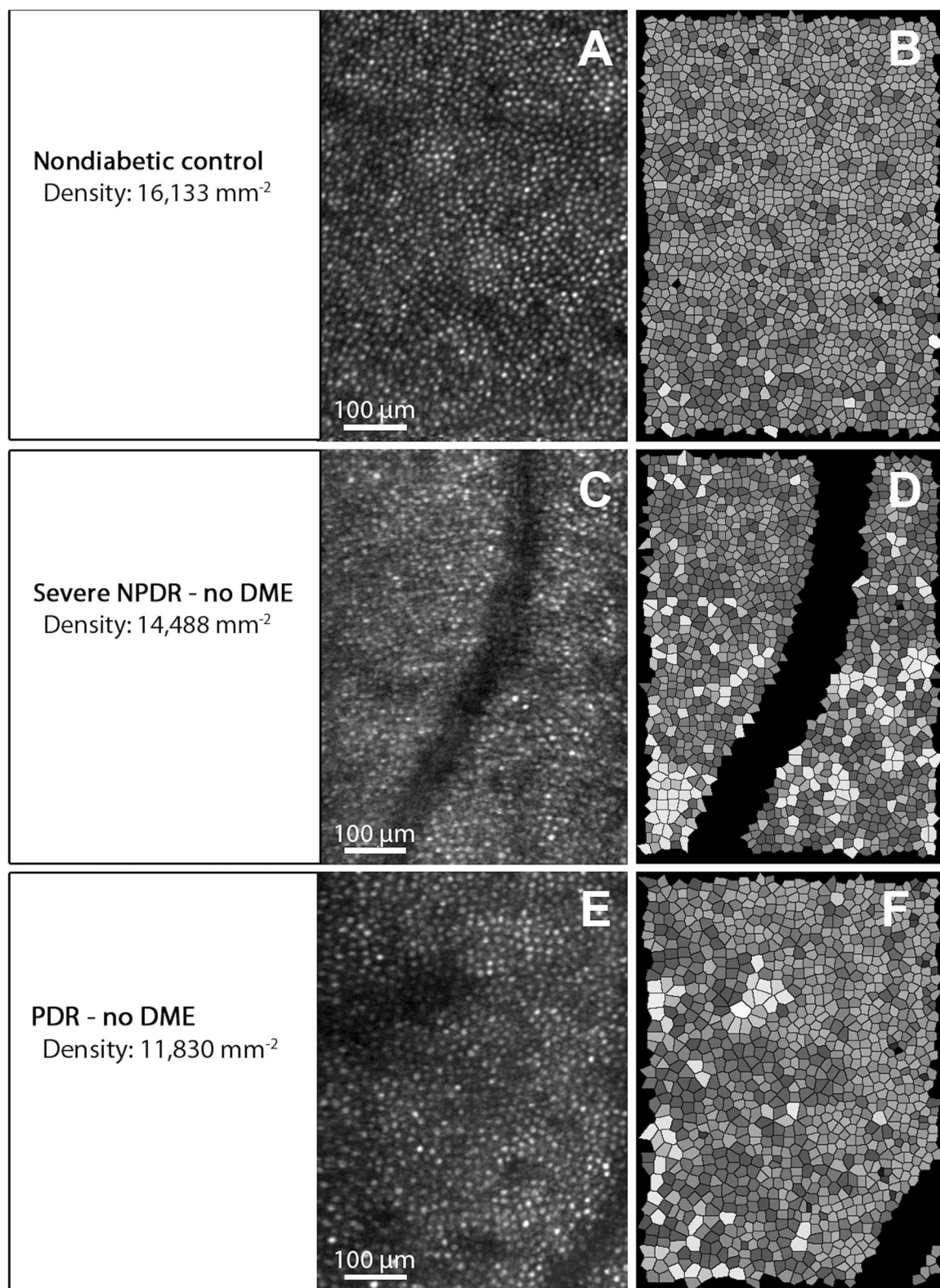


Fig. 5 Adaptive optics scanning laser ophthalmoscope (AO-SLO) imaging of photoreceptors in a healthy subject and diabetic patients. **a, c, e** Cone reflection images. **b, d, f** Voronoi analysis of cone photoreceptors in (**a, c, e**), respectively. Upper row: densely

packed cone photoreceptors in a healthy control subject. Middle and lower rows: reduced cone density and increased irregularity in the cone mosaic in patients with diabetic retinopathy. Reprinted with permission from Lammer et al. [152].

Age-related macular degeneration

In the developed world AMD is a leading cause of blindness. One application of AO in AMD is in monitoring retinal changes such as drusen, pigmentation, pseudodrusen and atrophy as well as changes in RPE and photoreceptors with progression of the disease (Fig. 6). One study demonstrated that cone photoreceptors are preserved over drusen in a patient with early onset large colloidal drusen [94].

Geographic atrophy has been studied using AO. Studies have looked at the changes in cone density at atrophic sites and in areas adjacent to these sites [95]. They showed that a complex, dynamic process of redistribution of hyporeflective clumps throughout the posterior pole precedes and accompanies the emergence and progression of atrophy. Hence these clumps are probable biomarkers of RPE damage and atrophy. As demonstrated here AO can be invaluable in measuring progression and in identifying those who may progress.

Furthermore, AO-SLO identified several small drusen deposits that were not observed with standard clinical imaging techniques leading to the potential of AMD being diagnosed at even earlier stages [96].

A study of photoreceptor distribution showed retinal cells overlying both soft and hard drusen exhibit structural and molecular abnormalities. These abnormalities resemble the degenerative effects confined to areas directly overlying drusen. This suggests that photoreceptor cell function is compromised as a consequence of drusen formation [97]. This has been shown in other studies using AO [98]. It is unclear which tissue is affected first in AMD: choroid, RPE, or photoreceptors. AO studies can help identify the time and the sequence in which tissues are affected first by identifying microscopic changes.

Finally, AO has been used in trials of AMD patients who have undergone stem cell therapy. Recently a team transplanted an autologous induced pluripotent stem cell-derived RPE cell sheet following removal of choroidal neovascularization in a patient with exudative age-related macular degeneration and polypoidal choroidal vasculopathy [99]. On follow up with AO dark cell-like structures (suspected to be RPE cells) with a predominantly hexagonal arrangement were observed in an area located near the margin of the graft sheet.

Inherited retinal dystrophies (IRD)

Inherited retinal degenerations have been investigated using AO. Table 2 shows the different types of IRD and the valuable information that has been obtained through the use of AO.

Glaucoma

There have been several studies looking at the use of AO in glaucoma. One study involved assessing the morphology of human lamina cribrosa pores in healthy and primary open-angle glaucoma (POAG) eyes. It concluded that on average, lamina cribrosa pores are elongated in POAG eyes and also in the healthy eyes of POAG relatives [100]. Another study looked at eyes with primary open-angle glaucoma who had suffered parafoveal visual field loss at least 3 years previously [101]. As determined using AO-SLO, eyes with glaucoma did not differ significantly from normal eyes in terms of cone density even in areas with visual field and/or nerve fibre loss. Although not many studies have been conducted with AO on glaucoma patients one study revealed the potential of this form of imaging by revealing glaucomatous damage that is difficult, if not impossible, to see with current OCT technology [102].

Other diseases

Given this relatively new form of imaging modality only a few studies have been conducted on other ophthalmic diseases. Examples of other eye diseases that were assessed using AO are summarised in Table 3.

Uses of adaptive optics

One of the main advantages of AO is its ability to detect changes at a microscopic level before macroscopic damage occurs. This can allow diseases to be detected earlier and therefore allowing a clinician the opportunity to intervene at an earlier stage in the disease process.

Furthermore, AO is capable of providing information immediately to researchers as opposed to histological samples post-mortem. AO provides us with further information on how the visual system i.e., the retina is organised in humans in both health and disease.

Once there is an expansion in volume of number of healthy and diseased AO imaging, we will be able to better and more efficiently identify and monitor ophthalmic disease using AO. A uniform way of measuring photoreceptor density and spacing should be established in order for all researchers/clinicians to carry out the above assessments in a standardised way and monitor the patient's disease using AO. Clinicians need to be taught how to interpret these images and given information on what AO images mean for their patient's condition.

AO can be used to determine what structures remain at the edge of lesions [22] i.e., the composition of cells. This is

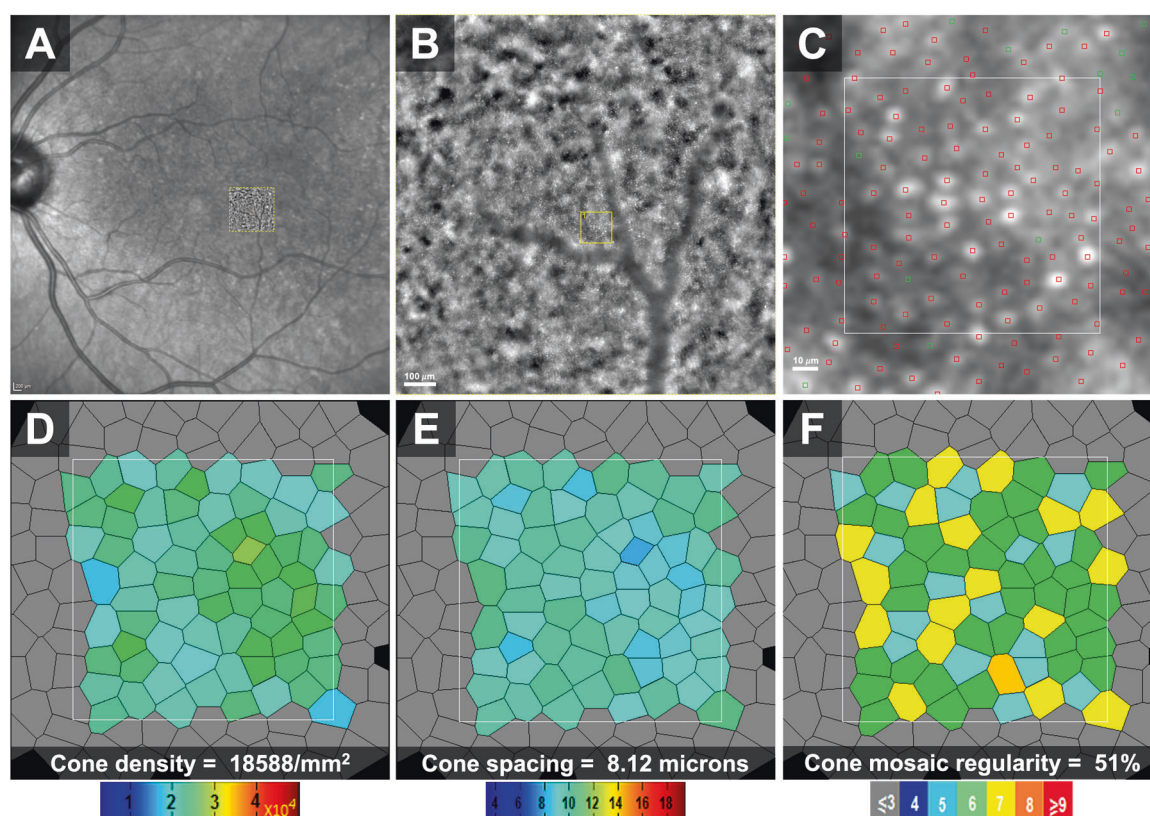


Fig. 6 Photoreceptor imaging in the left eye of a 71-year-old female patient with intermediate age-related macular degeneration. **a** A 30-degree *en face* infrared image with overlaid 4-degree adaptive optics flood illumination ophthalmoscope (AO-FIO) image (inside the red square). **b** The enlarged AO-FIO image of cone photoreceptor mosaic (4 degrees temporal to the centre of the fovea). The area

surrounded by a yellow square was enlarged for the qualitative analysis of cones. **c** Semiautomated detection of photoreceptors. Red squares correspond to automatically identified cones. Green squares represent cones that were manually corrected/identified. **d–f** Voronoi colour-coded maps of cone density, spacing and regularity, respectively.

particularly important when planning future therapies such as stem cell and gene therapies. AO permits observation of the natural history of retinal disease at a cellular level. This potentially could aid determining when a treatment could be instigated to maintain or improve vision to a patient.

Furthermore, phenotype determined by AO-SLO can be correlated with genotype to better understand inherited diseases such as Stargardt disease and retinitis pigmentosa. AO can be used to assess which cells/structures in the retina are affected in each disease/stage of disease helping us better target treatment. For example, one study demonstrated that cone photoreceptors are present in geographic atrophy without adjacent surviving RPE [103].

One future direction of AO is almost certainly in monitoring patients in clinical trials. AO can be used for participant selection, stratification and monitoring treatment safety and efficacy. AO has the advantage of being non-invasive and reproducible. It may identify early biomarkers of progression thus allowing shorter duration trials and novel clinical endpoints. This should accelerate drug development for retinal diseases. While AO use in clinical trials is still modest it has already been used to monitor

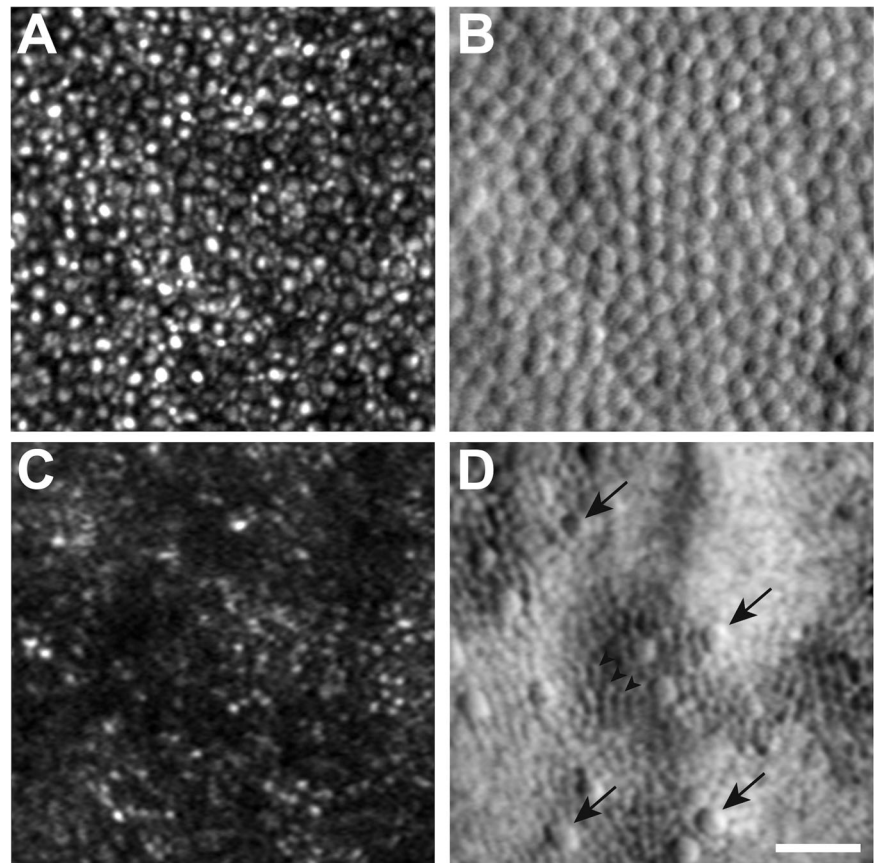
progression of retinitis pigmentosa in patients treated with ciliary neurotrophic factor (CNTF) [104]. More recent studies include a phase 2 multicentre randomized clinical trial of CNTF for macular telangiectasia type 2 [105] and a phase 1, open-label, safety and feasibility study of the implantation of human embryonic stem cell derived retinal pigment epithelium in subjects with acute wet AMD [106].

AO is undoubtedly an exceptional research tool given the high-quality and detailed images it can provide of the human retina. It enables resolution at a cellular level, but, the important question is what is its potential role in day to day clinical practice? To date AO has not been used routinely in clinical practice principally due to its high cost and complexity.

Adaptive optics in animal models and ex vivo tissue

Animal models play an important role in studying normal and diseased eyes. Classically, animal eyes have been studied in vitro using histopathological techniques, hindering

Fig. 7 Adaptive optics scanning laser ophthalmoscope (AO-SLO) imaging of photoreceptors at 5° temporal to the fovea from a healthy control (**a, b**) and a stargardt disease patient (**c, d**). Confocal (**a, c**) and split-detector (**b, d**) images clearly illustrates loss of cone photoreceptors in the patient as compared to the control. Black arrows in (**d**) represent some remaining cones. Scale bar: 25 μm . Reprinted with permission from Razeen et al. [153].



longitudinal assessment. Using AO for *in vivo* cellular imaging allows for non-invasive structural and functional investigations of the retina.

Non-human Old-World primates, especially the macaque monkey have been employed extensively as a model to understand structural and functional characteristics of the human retina. By using either endogenous or extrinsic fluorophores, single and multi-photon fluorescence AO-SLO systems were utilised to capture direct reflectance or fluorescence images of the microscopic structure of normal macaque retina, including RGC, photoreceptors, Müller cell processes, RPE, lamina cribrosa and microvasculature [42, 47, 107].

In vivo functional imaging has been accessible by using fluorescence AO in the primate eye. Morgan et al. used autofluorescence AO-SLO to characterise RPE damage and the reduction in retinal autofluorescence after light exposure to macaque retina [108]. Their experiments showed permanent retinal changes after using light conditions close to the maximum permissible exposure levels set by the American National Standards Institute (ANSI) [108]. In addition, Sincich et al. used AO-SLO to visualise and stimulate individual foveal cone photoreceptors to map the receptive field [109]. More recently, the retinoid cycle was investigated *in vivo* in the macaque by monitoring

fluorescence changes in photoreceptors during light and dark adaptation conditions [110]. The calcium response in RGC was also recorded after light stimulation [111].

The northern tree shrew is a mammal closely related to primates and has been recently used as a model in vision research. Sajdak et al. used a Shack-Hartman wavefront sensor to characterise the relatively high aberrations of the optical system of the tree shrew eye [112]. They adapted an AO-SLO instrument to image the cone photoreceptor mosaic using confocal and split-detection techniques. Sporadic rod photoreceptors were also visible on confocal and non-confocal images [112].

The mouse is the most commonly used animal model in biomedical research, including ophthalmic diseases. García de la Cera et al. used a Hartmann–Shack wavefront sensor to characterise optical aberrations in the mouse eye [113]. AO retinal imaging in the mouse can be more difficult than in human and non-human primates due to the smaller pupil size and the much thicker retina relative to the focal length of the mouse eye. One year later, Biss et al. used an AO system for *in vivo* and *ex vivo* imaging of fluorescently labelled retinal capillaries and microglial cells [114]. Fluorescent confocal AO-SLO has been also developed for the mouse eye with an average measured *in vivo* transverse and axial resolution of 0.79 μm and 10.8 μm ,

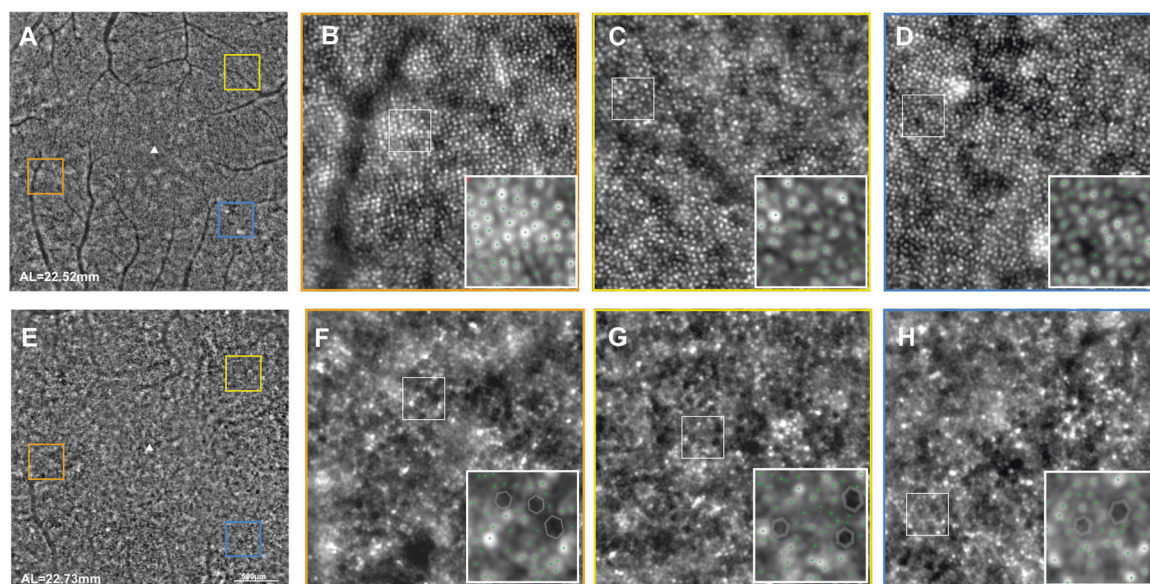


Fig. 8 Photoreceptor imaging in an age-matched normal subject (a–d) and a retinitis pigmentosa patient (e–h). **a, e** Central 10° AO image. Orange, yellow and blue squares correspond to the magnified images

in (b, f), (c, g) and (d, h), respectively. Decreased cone density and increased spacing can be detected in the patient. Reprinted with permission from Lin et al. [154].

Table 2 Examples of IRD assessed using AO.

Inherited Retinal Degeneration	Examples of findings in recent studies with AO
Stargardt's Disease	1. Increased cone and rod spacing in areas that appear normal in conventional images, suggesting that photoreceptor loss precedes clinically detectable retinal pigment epithelial disease in Stargardt's disease (Fig. 7) [141]. 2. AO-SLO in Stargardt's disease has shown abnormal and decreased photoreceptor density [141].
Retinitis Pigmentosa (RP)	3. In RP, cone photoreceptor cell loss occurred in the parafoveal region with a preserved ellipsoid zone/interdigitation zone (EZ/IZ) or visual sensitivity (Fig. 8) [142]. 4. AO used as an outcome measure to assess the photoreceptors in RP patients receiving ciliary neurotrophic factor [104].
Cone dystrophy	5. AOSLO imaging demonstrated variability in the pattern of cone and rod cell loss [143].
Best macular dystrophy	6. There is a significant cone photoreceptor loss in the macular region of patients with autosomal recessive bestrophinopathy, although the patients had relatively good visual acuity [144].
Bietti's crystalline dystrophy	7. There was a reduction in the cone count in all eyes in the area outside the outer retinal tubules [145].
Choroidal dystrophy	8. Parafoveal cone photoreceptors can be affected even at the early stage of central areolar choroidal dystrophy [146].

AO may also be useful for stratifying patients for inherited retinal disease trials. For example, in identifying patients with an adequate number of photoreceptors to be included in a study.

respectively [115]. The system allowed for direct non-invasive visualisation of nerve fibre bundles, blood vessels and photoreceptors. Fluorescently labelled ganglion cells and dendrites were also visualised and morphologically classified using the same system [115]. A similar instrument was modified for the use in rats [116]. With an average measured transverse resolution of 1.84 μm , images of microscopic structures in the rat retina were captured [116].

Yin et al. also utilised a similar fluorescent AO-SLO system to investigate the calcium response of individual ganglion cells after visual stimulation in mice expressing a

genetically encoded calcium indicator (G-CaMP3) [117]. Over the years, AO has been combined with several other imaging modalities for in vivo imaging of mice retina including OCT [14], two photon imaging [118] and multi-modal systems [119]. Due to the challenges faced with direct wavefront measurement in the eyes of small animals, an image-based AO approach has been recently proposed to measure and correct for aberrations without the need for wavefront sensor [120].

Recently, red blood cells and platelets were imaged within retinal capillaries using 2D confocal and split-

Table 3 Examples of eye diseases assessed using AO.

<i>Eye disease</i>	<i>Examples of findings in recent studies with AO</i>
Retinal detachment	Recovery of cone packing density measured by AO was associated with structural recovery of the outer retina observed in optical coherence tomography, suggesting regeneration of the photoreceptor outer segment after scleral buckle surgery for fovea-off rhegmatogenous retinal detachment [147].
Macula Hole	AO showing dark regions suggesting cone loss was seen in all eyes after macular hole repair. VA was better in eyes without dark regions at the centre of the fovea than in eyes with them [148].
Drug toxicity	Moderate cone loss was observed as hydroxychloroquine cumulative doses increased. The early detection of parafoveal cone metric changes may represent the earliest sign of hydroxychloroquine macular toxicity [149].
White dot syndrome	AO was used to quantify retinal photoreceptor density overlying lesions in various white dot syndromes. There was no statistically significant difference of photoreceptor density over active versus inactive lesions [150].
Vogt-Koyanagi-Harada (VKH)	Cone densities gradually increased after the resolution of serous retinal detachment in the eyes of VKH disease patients [151].

detector AO-SLO imaging [121]. 1D line scans orthogonal to a capillary enabled the calculation of cell flow velocity and capillary pulsatility. In addition, pericytes surrounding retinal capillary endothelial cells in transgenic mice were visualised using fluorescent AO-SLO [122].

AO imaging has recently been employed to characterise structural and functional changes as well as response to treatment in a mouse model of retinal diseases. AO-SLO detected shortened cone outer segments in the blue cone monochromacy mouse model, which was significantly restored after opsin gene augmentation therapy [123]. Functional fluorescent AO imaging also showed extensive functional loss in photoreceptor-degenerated *rd10* mice as compared to wild-type mice [124]. More recently, Miller et al. used multimodal imaging including AO-SLO to characterize short-term and long-term cellular interactions in the retina after focal photoreceptor damage [125].

Ex vivo imaging of biological specimens is also limited by wavefront aberrations from cellular/subcellular structures which can detriment image quality. AO has been combined with several microscopical approaches to enhance imaging quality and efficiency, thus reducing the needed illumination power. Two-photon excited fluorescence microscope uses two photons with a relatively long wavelength to excite intrinsic or extrinsic fluorophores to emit light which can then be detected to obtain 3D images. Debarre et al. incorporated an image-based sensor-less AO system to the microscope to provide depth-resolved aberration correction in biological samples [126]. Harmonic generation microscopy uses nonlinear optical properties to visualise tissue specimens. The variation in the generation of second or third harmonic radiation is used as a contrast to visualise cellular structure in three dimensions. AO was used to overcome the system- and specimen-induced aberrations, resulting in more efficient and higher resolution imaging [127]. Fluorescence fluctuation microscopy analyses the spatial and/or temporal fluctuation in fluorescence

signal to reveal morphological and functional characteristics of a biological tissue. AO has been able to measure and correct for single cell-induced aberrations allowing for more precise measurements [128]. Optical coherence microscopy combines the principles of OCT and confocal microscopy to produce 3D volumetric imaging of a biological specimen. Computational AO was utilised for real-time correction of aberrations to achieve a lateral resolution of 0.6 μm [129].

Limitations of adaptive optics

There are limitations to using AO in a clinical setting including the cost of running an AO imaging service, the time needed to scan patients, the lack of normative databases, the very small size of area imaged, and the quality of images obtained.

Firstly, good quality images cannot be obtained readily in a significant number of patients due to optical media densities/abnormalities such as dry eyes, cataracts, vitreous debris and corneal scarring. In addition, large/uncontrolled eye movements such as nystagmus can also further depreciate the quality of the images obtained. The quality of the images also depends on how well the patient cooperates and it may be difficult to achieve good cooperation from elderly patients whom make up the majority of patients seen in ophthalmology clinics. If good quality scans cannot be obtained in a timely manner in a clinic setting it will mean this form of imaging may not be so readily introduced for clinical use.

Another limitation of AO is the number of degrees from the fovea which the photoreceptors have been imaged. Photoreceptors (rods and cones) have been imaged out to 30° in the temporal and nasal retina [130]. This is particularly important in studying conditions affecting the peripheral retina such as retinitis pigmentosa. The field of view and the reach of the camera to the peripheral retina needs to

be enhanced in order to be able to assess monitor and analyse more peripheral regions. The field of view is very narrow in AO meaning that re-imaging the same area will be necessary for comparative purposes e.g., cone receptor densities in two different areas of the retina done at different times will not be comparable. Given the small area imaged, pathology in other areas of the retina may be missed.

Given the high cost of AO devices eye units will need a sufficient clinical indication in order to purchase this expensive device. Several companies have developed AO prototypes including Boston Micromachines Corporation, Canon, Inc., Imagine Eyes and Physical Sciences, Inc. However, very few machines have regulatory approval.

As mentioned previously the images produced are complex and normative databases are lacking. For AO to be useful at the very least normative, data bases need to be produced and clinicians need to be trained in interpreting these.

Finally, AO provides us with structural information, and it is difficult to determine whether this correlates with function i.e., healthy appearing cones/rods may in fact not be functioning despite normal structural appearance or vice versa. Again, further research needs to be done before this can be established.

Future of adaptive optics

The use of AO technology for retinal imaging has been growing exponentially since its introduction to vision research by the end of last century. However, the previously mentioned limitations curbed its expansion into widespread clinical utilisation. Efforts are being made to overcome some of these challenges. The analysis of AO images is complex, laborious and time-consuming. Automated algorithms, including machine learning techniques, might offer a more robust alternative to manual grading [131]. Proper validation and reliability assessment of these automated algorithms are needed to characterise their performance. A wide range of AO metrics are being used by different research groups. Standardisation of the nomenclature and definition of AO metrics might be needed.

Continuous advancements in AO hardware and software will reduce the size and cost of AO imaging systems. Sensorless AO systems have been developed to use the image itself, rather than a wavefront sensor, to measure and correct the aberrations [132]. Computational AO is another technique that measures the amplitude and phase of the back scattered light to calculate and minimise the effect of wavefront aberrations [133]. These techniques can simplify the hardware needed for an AO system, and potentially cut the costs. Although the image quality might not be as good

as a conventional full hardware system, reasonable trade-offs are often needed to achieve a manageable cost.

Other technical improvements are making the technology easier to use. These include increased imaging speeds and the use of eye-tracking systems to significantly eliminate the effect of motion artefacts [134]. Several approaches have also been recently introduced to maximise the corrected field of view of AO systems. Multi-pupil AO and conjugate AO with multiple guide stars approaches have been described for simultaneous aberration correction over a wider area [135, 136]. More recently, Camino et al. developed a hill-climbing algorithm for real-time estimation of the largest achievable field of view in an AO-OCT system [137]. Increased computational speeds and parallel processing capabilities will continue to enhance the efficiency and capacity of AO imaging.

Non-confocal AO imaging has also been an emerging area of interest over the last several years [138]. Further work is needed to better understand the images and to determine their association with retinal structure and function. AO-OCT and AO-OCT angiography are showing great potential for 3D visualisation of the neurosensory retina, as well as choroidal and retinal vascular networks [29, 139]. More recently, AO was combined with swept-source OCT to achieve deeper tissue penetration [133]. In addition, fluorescence imaging techniques have been described in humans and animals for enhanced visualisation of retinal cells and microvasculature [140]. Two-photon excitation fluorescence has also been widely used in animal models to capture high-contrast images of retinal structure [47]. However, more work is needed to optimise light exposure for human use.

In summary, AO offers the ability to image the retina at a cellular level in vivo. As its use widens it offers the opportunity to better understand the pathogenesis of retinal disease. Similar to the first ophthalmoscopes, there are technical challenges in using AO. However, as the technology develops and it becomes easier to use it should play an increasing role in clinical management and clinical trials leading to better outcomes for patients.

Funding This research was funded by Wellcome Trust grant number 210572/Z/18/Z, an NIHR senior investigator award to AL and the National Institute for Health Research (NIHR) Biomedical Research Centre based at Moorfields Eye Hospital NHS Foundation Trust and UCL Institute of Ophthalmology.

Compliance with ethical standards

Conflict of interest The authors declare that they have no conflict of interest.

Publisher's note Springer Nature remains neutral with regard to jurisdictional claims in published maps and institutional affiliations.

References

- Miller DT, Williams DR, Morris GM, Liang J. Images of cone photoreceptors in the living human eye. *Vis Res*. 1996;36:1067–79.
- Wade A, Fitzke F. A fast, robust pattern recognition asystem for low light level image registration and its application to retinal imaging. *Opt Express*. 1998;3:190–7.
- Huang D, Swanson EA, Lin CP, Schuman JS, Stinson WG, Chang W, et al. Optical coherence tomography. *Science*. 1991;254:1178–81.
- Babcock HW. The possibility of compensating astronomical seeing. *Publ Astronomical Soc Pac*. 1953;65:229–36.
- Dreher AW, Bille JF, Weinreb RN. Active optical depth resolution improvement of the laser tomographic scanner. *Appl Opt*. 1989;28:804–8.
- Liang J, Williams DR, Miller DT. Supernormal vision and high-resolution retinal imaging through adaptive optics. *J Opt Soc Am A Opt Image Sci Vis*. 1997;14:2884–92.
- Roorda A. Adaptive optics ophthalmoscopy. *J Refract Surg*. 2000;16:S602–7.
- Cooper RF, Dubis AM, Pavaskar A, Rha J, Dubra A, Carroll J. Spatial and temporal variation of rod photoreceptor reflectance in the human retina. *Biomed Opt Express*. 2011;2:2577–89.
- Roorda A, Romero-Borja F, Donnelly Iii W, Queener H, Hebert T, Campbell M. Adaptive optics scanning laser ophthalmoscopy. *Opt Express*. 2002;10:405–12.
- Liang J, Grimm B, Goelz S, Bille JF. Objective measurement of wave aberrations of the human eye with the use of a Hartmann-Shack wave-front sensor. *J Opt Soc Am A Opt Image Sci Vis*. 1994;11:1949–57.
- Ragazzoni R. Pupil plane wavefront sensing with an oscillating prism. *J Mod Opt*. 1996;43:289–93.
- Fernández EJ, Povazay B, Hermann B, Unterhuber A, Sattmann H, Prieto PM, et al. Three-dimensional adaptive optics ultrahigh-resolution optical coherence tomography using a liquid crystal spatial light modulator. *Vis Res*. 2005;45:3432–44.
- Jian Y, Zawadzki RJ, Sarunic MV. Adaptive optics optical coherence tomography for in vivo mouse retinal imaging. *J Biomed Opt*. 2013;18:56007.
- Jian Y, Xu J, Gradowski MA, Bonora S, Zawadzki RJ, Sarunic MV. Wavefront sensorless adaptive optics optical coherence tomography for in vivo retinal imaging in mice. *Biomed Opt Express*. 2014;5:547–59.
- Elsner AE, Burns SA, Weiter JJ, Delori FC. Infrared imaging of sub-retinal structures in the human ocular fundus. *Vis Res*. 1996;36:191–205.
- Lombardo M, Serrao S, Ducoli P, Lombardo G. Variations in image optical quality of the eye and the sampling limit of resolution of the cone mosaic with axial length in young adults. *J Cataract Refract Surg*. 2012;38:1147–55.
- Querques G, Kamami-Levy C, Georges A, Pedinielli A, Capuano V, Blanco-Garavito R, et al. Adaptive optics imaging of foveal sparing in geographic atrophy secondary to age-related macular degeneration. *Retina*. 2016;36:247–54.
- Meixner E, Michelson G. Measurement of retinal wall-to-lumen ratio by adaptive optics retinal camera: a clinical research. *Graefes Arch Clin Exp Ophthalmol*. 2015; 253:1985–95.
- Tumahai P, Moureaux C, Meillat M, Debellemanniere G, Flores M, Delbosc B, et al. High-resolution imaging of photoreceptors in healthy human eyes using an adaptive optics retinal camera. *Eye (Lond)*. 2018;32:1723–30.
- Webb RH, Hughes GW, Delori FC. Confocal scanning laser ophthalmoscope. *Appl Opt*. 1987;26:1492–9.
- Burns SA, Elsner AE, Sapoznik KA, Warner RL, Gast TJ. Adaptive optics imaging of the human retina. *Prog Retin Eye Res*. 2019;68:1–30.
- Dubis AM, Cooper RF, Aboshiha J, Langlo CS, Sundaram V, Liu B, et al. Genotype-dependent variability in residual cone structure in achromatopsia: toward developing metrics for assessing cone health. *Invest Ophthalmol Vis Sci*. 2014;55:7303–11.
- Liu Z, Kurokawa K, Zhang F, Lee JJ, Miller DT. Imaging and quantifying ganglion cells and other transparent neurons in the living human retina. *Proc Natl Acad Sci USA*. 2017;114:12803–8.
- Scoles D, Sulai YN, Dubra A. In vivo dark-field imaging of the retinal pigment epithelium cell mosaic. *Biomed Opt Express*. 2013;4:1710–23.
- Scoles D, Sulai YN, Langlo CS, Fishman GA, Curcio CA, Carroll J, et al. In vivo imaging of human cone photoreceptor inner segments. *Invest Ophthalmol Vis Sci*. 2014;55:4244–51.
- Fernandez E, Drexler W. Influence of ocular chromatic aberration and pupil size on transverse resolution in ophthalmic adaptive optics optical coherence tomography. *Opt Express*. 2005;13:8184–97.
- Zhang Y, Rha J, Jonnal R, Miller D. Adaptive optics parallel spectral domain optical coherence tomography for imaging the living retina. *Opt Express*. 2005;13:4792–811.
- Zawadzki RJ, Jones SM, Olivier SS, Zhao M, Bower BA, Izatt JA, et al. Adaptive-optics optical coherence tomography for high-resolution and high-speed 3D retinal in vivo imaging. *Opt Express*. 2005;13:8532–46.
- Dong ZM, Wollstein G, Wang B, Schuman JS. Adaptive optics optical coherence tomography in glaucoma. *Prog Retin Eye Res*. 2017;57:76–88.
- Curcio CA, Sloan KR, Kalina RE, Hendrickson AE. Human photoreceptor topography. *J Comp Neurol*. 1990;292:497–523.
- Li KY, Roorda A. Automated identification of cone photoreceptors in adaptive optics retinal images. *J Opt Soc Am A Opt Image Sci Vis*. 2007;24:1358–63.
- Bergeles C, Dubis AM, Davidson B, Kasilian M, Kalitzeos A, Carroll J, et al. Unsupervised identification of cone photoreceptors in non-confocal adaptive optics scanning light ophthalmoscope images. *Biomed Opt Express*. 2017;8:3081–94.
- Litts KM, Cooper RF, Duncan JL, Carroll J. Photoreceptor-based biomarkers in AOSLO retinal imaging. *Invest Ophthalmol Vis Sci*. 2017;58:BIO255–67.
- Garrioch R, Langlo C, Dubis AM, Cooper RF, Dubra A, Carroll J. Repeatability of in vivo parafoveal cone density and spacing measurements. *Optom Vis Sci*. 2012;89:632–43.
- Cooper RF, Wilk MA, Tarima S, Carroll J. Evaluating descriptive metrics of the human cone mosaic. *Invest Ophthalmol Vis Sci*. 2016;57:2992–3001.
- Cooper RF, Lombardo M, Carroll J, Sloan KR, Lombardo G. Methods for investigating the local spatial anisotropy and the preferred orientation of cones in adaptive optics retinal images. *Vis Neurosci*. 2016;33:E005.
- Liu J, Jung H, Dubra A, Tam J. Cone photoreceptor cell segmentation and diameter measurement on adaptive optics images using circularly constrained active contour model. *Invest Ophthalmol Vis Sci*. 2018;59:4639–52.
- Jonnal RS, Kocaoglu OP, Wang Q, Lee S, Miller DT. Phase-sensitive imaging of the outer retina using optical coherence tomography and adaptive optics. *Biomed Opt Express*. 2012;3:104–24.
- Pallikaris A, Williams DR, Hofer H. The reflectance of single cones in the living human eye. *Invest Ophthalmol Vis Sci*. 2003;44:4580–92.

40. Duncan JL, Roorda A. Dysflective cones. *Adv Exp Med Biol.* 2019;1185:133–7.
41. Bruce KS, Harmening WM, Langston BR, Tuten WS, Roorda A, Sincich LC. Normal perceptual sensitivity arising from weakly reflective cone photoreceptors. *Invest Ophthalmol Vis Sci.* 2015;56:4431–8.
42. Morgan JJ, Dubra A, Wolfe R, Merigan WH, Williams DR. In vivo autofluorescence imaging of the human and macaque retinal pigment epithelial cell mosaic. *Invest Ophthalmol Vis Sci.* 2009;50:1350–9.
43. Roorda A, Zhang Y, Duncan JL. High-resolution in vivo imaging of the RPE mosaic in eyes with retinal disease. *Invest Ophthalmol Vis Sci.* 2007;48:2297–303.
44. Liu T, Jung H, Liu J, Droettboom M, Tam J. Noninvasive near infrared autofluorescence imaging of retinal pigment epithelial cells in the human retina using adaptive optics. *Biomed Opt Express.* 2017;8:4348–60.
45. Granger CE, Yang Q, Song H, Saito K, Nozato K, Latchney LR, et al. Human retinal pigment epithelium: in vivo cell morphometry, multispectral autofluorescence, and relationship to cone mosaic. *Invest Ophthalmol Vis Sci.* 2018;59:5705–16.
46. Liu Z, Kurokawa K, Hammer DX, Miller DT. In vivo measurement of organelle motility in human retinal pigment epithelial cells. *Biomed Opt Express.* 2019;10:4142–58.
47. Rossi EA, Granger CE, Sharma R, Yang Q, Saito K, Schwarz C, et al. Imaging individual neurons in the retinal ganglion cell layer of the living eye. *Proc Natl Acad Sci USA.* 2017;114:586–91.
48. Ivers KM, Li C, Patel N, Sredar N, Luo X, Queener H, et al. Reproducibility of measuring lamina cribrosa pore geometry in human and nonhuman primates with in vivo adaptive optics imaging. *Invest Ophthalmol Vis Sci.* 2011;52:5473–80.
49. Bennett AG, Rudnicka AR, Edgar DF. Improvements on Littmann's method of determining the size of retinal features by fundus photography. *Graefes Arch Clin Exp Ophthalmol.* 1994;32:361–7.
50. Nadler Z, Wang B, Schuman JS, Ferguson RD, Patel A, Hammer DX, et al. In vivo three-dimensional characterization of the healthy human lamina cribrosa with adaptive optics spectral-domain optical coherence tomography. *Invest Ophthalmol Vis Sci.* 2014;55:6459–66.
51. Bedggood P, Metha A. Adaptive optics imaging of the retinal microvasculature. *Clin Exp Optom.* 2020;103:112–22.
52. Chui TY, Gast TJ, Burns SA. Imaging of vascular wall fine structure in the human retina using adaptive optics scanning laser ophthalmoscopy. *Invest Ophthalmol Vis Sci.* 2013;54:7115–24.
53. Burns SA, Elsner AE, Chui TY, Vannasdale DA Jr., Clark CA, Gast TJ, et al. In vivo adaptive optics microvascular imaging in diabetic patients without clinically severe diabetic retinopathy. *Biomed Opt Express.* 2014;5:961–74.
54. Hillard JG, Gast TJ, Chui TY, Sapir D, Burns SA. Retinal arterioles in hypo-, normo-, and hypertensive subjects measured using adaptive optics. *Transl Vis Sci Technol.* 2016;5:16.
55. Luo T, Gast TJ, Vermeer TJ, Burns SA. Retinal vascular branching in healthy and diabetic subjects. *Invest Ophthalmol Vis Sci.* 2017;58:2685–94.
56. Tam J, Martin JA, Roorda A. Noninvasive visualization and analysis of parafoveal capillaries in humans. *Invest Ophthalmol Vis Sci.* 2010;51:1691–8.
57. Chui TYP, Mo S, Krawitz B, Menon NR, Choudhury N, Gan A, et al. Human retinal microvascular imaging using adaptive optics scanning light ophthalmoscopy. *Int J Retin Vitreous.* 2016;2:11.
58. Tam J, Dhamdhare KP, Tiruveedhula P, Manzanera S, Barez S, Bearse MA Jr., et al. Disruption of the retinal parafoveal capillary network in type 2 diabetes before the onset of diabetic retinopathy. *Invest Ophthalmol Vis Sci.* 2011;52:9257–66.
59. Tsujikawa A, Ogura Y. Evaluation of leukocyte-endothelial interactions in retinal diseases. *Ophthalmologica.* 2012;227:68–79.
60. Martin JA, Roorda A. Direct and noninvasive assessment of parafoveal capillary leukocyte velocity. *Ophthalmology.* 2005;112:2219–24.
61. Lu Y, Bernabeu MO, Lammer J, Cai CC, Jones ML, Franco CA, et al. Computational fluid dynamics assisted characterization of parafoveal hemodynamics in normal and diabetic eyes using adaptive optics scanning laser ophthalmoscopy. *Biomed Opt Express.* 2016;7:4958–73.
62. Martin JA, Roorda A. Pulsatility of parafoveal capillary leukocytes. *Exp Eye Res.* 2009;88:356–60.
63. Tam J, Tiruveedhula P, Roorda A. Characterization of single-file flow through human retinal parafoveal capillaries using an adaptive optics scanning laser ophthalmoscope. *Biomed Opt Express.* 2011;2:781–93.
64. Zhong Z, Petrig BL, Qi X, Burns SA. In vivo measurement of erythrocyte velocity and retinal blood flow using adaptive optics scanning laser ophthalmoscopy. *Opt Express.* 2008;16:12746–56.
65. Zhong Z, Song H, Chui TY, Petrig BL, Burns SA. Noninvasive measurements and analysis of blood velocity profiles in human retinal vessels. *Invest Ophthalmol Vis Sci.* 2011;52:4151–7.
66. Palochak CMA, Lee HE, Song J, Geng A, Linsenmeier RA, Burns SA, et al. Retinal Blood Velocity and Flow in Early Diabetes and Diabetic Retinopathy Using Adaptive Optics Scanning Laser Ophthalmoscopy. *J Clin Med.* 2019;8:8.
67. Harmening WM, Sincich LC. Adaptive optics for photoreceptor-targeted psychophysics. In: Bille JF, editor. *High resolution imaging in microscopy and ophthalmology: new frontiers in biomedical optics.* Cham (CH); 2019. pp. 359–75.
68. Hofer H, Carroll J, Neitz J, Neitz M, Williams DR. Organization of the human trichromatic cone mosaic. *J Neurosci.* 2005;25:9669–79.
69. Grieve K, Roorda A. Intrinsic signals from human cone photoreceptors. *Invest Ophthalmol Vis Sci.* 2008;49:713–9.
70. Hillmann D, Spahr H, Pfaffle C, Sudkamp H, Franke G, Hutmacher G. In vivo optical imaging of physiological responses to photostimulation in human photoreceptors. *Proc Natl Acad Sci USA.* 2016;113:13138–43.
71. Litts KM, Wang X, Clark ME, Owsley C, Freund KB, Curcio CA, et al. Exploring photoreceptor reflectivity through multimodal imaging of outer retinal tubulation in advanced age-related macular degeneration. *Retina.* 2017;37:978–88.
72. Panorgias A, Zawadzki RJ, Capps AG, Hunter AA, Morse LS, Werner JS. Multimodal assessment of microscopic morphology and retinal function in patients with geographic atrophy. *Invest Ophthalmol Vis Sci.* 2013;54:4372–84.
73. Wang Q, Tuten WS, Lujan BJ, Holland J, Bernstein PS, Schwartz SD, et al. Adaptive optics microperimetry and OCT images show preserved function and recovery of cone visibility in macular telangiectasia type 2 retinal lesions. *Invest Ophthalmol Vis Sci.* 2015;56:778–86.
74. Kocaoglu OP, Liu Z, Zhang F, Kurokawa K, Jonnal RS, Miller DT. Photoreceptor disc shedding in the living human eye. *Biomed Opt Express.* 2016;7:4554–68.
75. Sabesan R, Schmidt BP, Tuten WS, Roorda A. The elementary representation of spatial and color vision in the human retina. *Sci Adv.* 2016;2:e1600797.
76. Yang Q, Arathorn DW, Tiruveedhula P, Vogel CR, Roorda A. Design of an integrated hardware interface for AOSLO image capture and cone-targeted stimulus delivery. *Opt Express.* 2010;18:17841–58.
77. Tuten WS, Harmening WM, Sabesan R, Roorda A, Sincich LC. Spatiochromatic Interactions between Individual Cone Photoreceptors in the Human Retina. *J Neurosci.* 2017;37:9498–509.

78. Duan A, Bedggood PA, Bui BV, Metha AB. Evidence of flicker-induced functional hyperaemia in the smallest vessels of the human retinal blood supply. *PLoS ONE*. 2016;11:e0162621.
79. Newman EA. Functional hyperemia and mechanisms of neurovascular coupling in the retinal vasculature. *J Cereb Blood Flow Metab*. 2013;33:1685–95.
80. Duan A, Bedggood PA, Metha AB, Bui BV. Reactivity in the human retinal microvasculature measured during acute gas breathing provocations. *Sci Rep*. 2017;7:2113.
81. Hagag AM, Pechauer AD, Liu L, Wang J, Zhang M, Jia Y, et al. OCT angiography changes in the 3 parafoveal retinal plexuses in response to hyperoxia. *Ophthalmol Retina*. 2018;2:329–36.
82. Song H, Chui TY, Zhong Z, Elsner AE, Burns SA. Variation of cone photoreceptor packing density with retinal eccentricity and age. *Invest Ophthalmol Vis Sci*. 2011;52:7376–84.
83. Park SP, Chung JK, Greenstein V, Tsang SH, Chang S. A study of factors affecting the human cone photoreceptor density measured by adaptive optics scanning laser ophthalmoscope. *Exp Eye Res*. 2013;108:1–9.
84. Zaleska-Zmijewska A, Wawrzyniak ZM, Ulinska M, Szaflik J, Dabrowska A, Szaflik JP. Human photoreceptor cone density measured with adaptive optics technology (rtx1 device) in healthy eyes: standardization of measurements. *Med (Baltim)*. 2017;96:e7300.
85. Lombardo M, Parravano M, Lombardo G, Varano M, Boccassini B, Stirpe M, et al. Adaptive optics imaging of parafoveal cones in type 1 diabetes. *Retina*. 2014;34:546–57.
86. Tam J, Dhamdhare KP, Tiruveedhula P, Manzanera S, Barez S, Bearse MA Jr., et al. Disruption of the retinal parafoveal capillary network in type 2 diabetes before the onset of diabetic retinopathy. *Investigative Ophthalmol Vis Sci*. 2011;52:9257–66.
87. Sun JK, Prager S, Radwan S, Ramsey DJ, Silva PS, Kwak H, et al. Photoreceptor mosaic changes in diabetic eye disease assessed by adaptive optics scanning laser ophthalmoscopy (AOSLO). *Investigative Ophthalmol Vis Sci*. 2012;53:4647.
88. Tan W, Wright T, Rajendran D, Garcia-Sanchez Y, Finkelberg L, Ksilak M, et al. Cone-photoreceptor density in adolescents with type 1 diabetes. *Invest Ophthalmol Vis Sci*. 2015;56:6339–43.
89. Lombardo M, Parravano M, Serrao S, Ducoli P, Stirpe M, Lombardo G. Analysis of retinal capillaries in patients with type 1 diabetes and nonproliferative diabetic retinopathy using adaptive optics imaging. *Retina*. 2013;33:1630–9.
90. Chui TY, Dubow N, Pinhas A, Shah N, Gan A, Weitz R, et al. Comparison of adaptive optics scanning light ophthalmoscopic fluorescein angiography and offset pinhole imaging. *Biomed Opt Express*. 2014;5:1173–89.
91. Meirelles ALB, Rodrigues MW, Guirado AF, Jorge R. Photoreceptor assessment using adaptive optics in resolved central serous chorioretinopathy. *Arq Bras Oftalmol*. 2017;80:192–5.
92. Ooto S, Hangai M, Sakamoto A, Tsujikawa A, Yamashiro K, Ojima Y, et al. High-resolution imaging of resolved central serous chorioretinopathy using adaptive optics scanning laser ophthalmoscopy. *Ophthalmology*. 2010;117:1800–9.e2.
93. Nakamura T, Ueda-Consolvo T, Oiwake T, Hayashi A. Correlation between outer retinal layer thickness and cone density in patients with resolved central serous chorioretinopathy. *Graefes Arch Clin Exp Ophthalmol*. 2016;254:2347–54.
94. Querques G, Massamba N, Guigui B, Lea Q, Lamory B, Soubrane G, et al. In vivo evaluation of photoreceptor mosaic in early onset large colloid drusen using adaptive optics. *Acta Ophthalmol*. 2012;90:e327–8.
95. Gocho K, Sarda V, Falah S, Sahel J-A, Sennlaub F, Benchaboune M, et al. Adaptive optics imaging of geographic atrophy. *Investigative Ophthalmol Vis Sci*. 2013;54:3673–80.
96. Boretzky A, Khan F, Burnett G, Hammer DX, Ferguson RD, van Kuijk F, et al. In vivo imaging of photoreceptor disruption associated with age-related macular degeneration: a pilot study. *Lasers Surg Med*. 2012;44:603–10.
97. Johnson PT, Lewis GP, Talaga KC, Brown MN, Kappel PJ, Fisher SK, et al. Drusen-associated degeneration in the retina. *Invest Ophthalmol Vis Sci*. 2003;44:4481–8.
98. Godara P, Siebe C, Rha J, Michaelides M, Carroll J. Assessing the photoreceptor mosaic over drusen using adaptive optics and SD-OCT. *Ophthalmic Surg Lasers Imaging*. 2010;41:S104–8.
99. Takagi S, Mandai M, Gocho K, Hiram Y, Yamamoto M, Fujihara M, et al. Evaluation of transplanted autologous induced pluripotent stem cell-derived retinal pigment epithelium in exudative age-related macular degeneration. *Ophthalmol Retina*. 2019;3:850–9.
100. Zwillingner S, Paques M, Safran B, Baudouin C. In vivo characterization of lamina cribrosa pore morphology in primary open-angle glaucoma. *J Fr Ophtalmol*. 2016;39:265–71.
101. Hasegawa T, Ooto S, Takayama K, Makiyama Y, Akagi T, Ikeda HO, et al. Cone integrity in glaucoma: an adaptive-optics scanning laser ophthalmoscopy study. *Am J Ophthalmol*. 2016;171:53–66.
102. Chen MF, Chui TYP, Alhadeff P, Rosen RB, Ritch R, Dubra A, et al. Adaptive optics imaging of healthy and abnormal regions of retinal nerve fiber bundles of patients with glaucoma. *Investigative Ophthalmol Vis Sci*. 2015;56:674–81.
103. King BJ, Sapoznik KA, Elsner AE, Gast TJ, Papay JA, Clark CA, et al. SD-OCT and adaptive optics imaging of outer retinal tubulation. *Optom Vis Sci*. 2017;94:411–22.
104. Talcott KE, Ratnam K, Sundquist SM, Lucero AS, Lujan BJ, Tao W, et al. Longitudinal study of cone photoreceptors during retinal degeneration and in response to ciliary neurotrophic factor treatment. *Invest Ophthalmol Vis Sci*. 2011;52:2219–26.
105. Loo J, Clemons TE, Chew EY, Friedlander M, Jaffe GJ, Farsiu S. Beyond performance metrics: automatic deep learning retinal OCT analysis reproduces clinical trial outcome. *Ophthalmology*. 2020;127:793–801.
106. da Cruz L, Fynes K, Georgiadis O, Kerby J, Luo YH, Ahmado A, et al. Phase 1 clinical study of an embryonic stem cell-derived retinal pigment epithelium patch in age-related macular degeneration. *Nat Biotechnol*. 2018;36:328–37.
107. Sharma R, Williams DR, Palczewska G, Palczewski K, Hunter JJ. Two-photon autofluorescence imaging reveals cellular structures throughout the retina of the living primate eye. *Invest Ophthalmol Vis Sci*. 2016;57:632–46.
108. Morgan JJ, Hunter JJ, Masella B, Wolfe R, Gray DC, Merigan WH, et al. Light-induced retinal changes observed with high-resolution autofluorescence imaging of the retinal pigment epithelium. *Invest Ophthalmol Vis Sci*. 2008;49:3715–29.
109. Sincich LC, Zhang Y, Tiruveedhula P, Horton JC, Roorda A. Resolving single cone inputs to visual receptive fields. *Nat Neurosci*. 2009;12:967–9.
110. Sharma R, Schwarz C, Williams DR, Palczewska G, Palczewski K, Hunter JJ. In vivo two-photon fluorescence kinetics of primate rods and cones. *Invest Ophthalmol Vis Sci*. 2016;57:647–57.
111. Yin L, Masella B, Dalkara D, Zhang J, Flannery JG, Schaffer DV, et al. Imaging light responses of foveal ganglion cells in the living macaque eye. *J Neurosci*. 2014;34:6596–605.
112. Sajdak BS, Salmon AE, Cava JA, Allen KP, Freling S, Ramamirtham R, et al. Noninvasive imaging of the tree shrew eye: Wavefront analysis and retinal imaging with correlative histology. *Exp Eye Res*. 2019;185:107683.
113. de la Cera EG, Rodriguez G, Llorente L, Schaeffel F, Marcos S. Optical aberrations in the mouse eye. *Vis Res*. 2006;46:2546–53.

114. Biss DP, Sumorok D, Burns SA, Webb RH, Zhou Y, Bifano TG, et al. In vivo fluorescent imaging of the mouse retina using adaptive optics. *Opt Lett*. 2007;32:659–61.
115. Geng Y, Dubra A, Yin L, Merigan WH, Sharma R, Libby RT, et al. Adaptive optics retinal imaging in the living mouse eye. *Biomed Opt Express*. 2012;3:715–34.
116. Geng Y, Greenberg KP, Wolfe R, Gray DC, Hunter JJ, Dubra A, et al. In vivo imaging of microscopic structures in the rat retina. *Invest Ophthalmol Vis Sci*. 2009;50:5872–9.
117. Yin L, Geng Y, Osakada F, Sharma R, Cetin AH, Callaway EM, et al. Imaging light responses of retinal ganglion cells in the living mouse eye. *J Neurophysiol*. 2013;109:2415–21.
118. Palczewska G, Dong Z, Golczak M, Hunter JJ, Williams DR, Alexander NS, et al. Noninvasive two-photon microscopy imaging of mouse retina and retinal pigment epithelium through the pupil of the eye. *Nat Med*. 2014;20:785–9.
119. Hammer DX, Ferguson RD, Mujat M, Patel A, Plumb E, Iftimia N, et al. Multimodal adaptive optics retinal imager: design and performance. *J Opt Soc Am A Opt Image Sci Vis*. 2012;29:2598–607.
120. Wahl DJ, Zhang P, Mocci J, Quintavalla M, Muradore R, Jian Y, et al. Adaptive optics in the mouse eye: wavefront sensing based vs. image-guided aberration correction. *Biomed Opt Express*. 2019;10:4757–74.
121. Joseph A, Guevara-Torres A, Schallek J. Imaging single-cell blood flow in the smallest to largest vessels in the living retina. *Elife*. 2019;8:1–36.
122. Schallek J, Geng Y, Nguyen H, Williams DR. Morphology and topography of retinal pericytes in the living mouse retina using in vivo adaptive optics imaging and ex vivo characterization. *Invest Ophthalmol Vis Sci*. 2013;54:8237–50.
123. Deng WT, Li J, Zhu P, Chiodo VA, Smith WC, Freedman B, et al. Human L- and M-opsins restore M-cone function in a mouse model for human blue cone monochromacy. *Mol Vis*. 2018;24:17–28.
124. Cheong SK, Strazzeri JM, Williams DR, Merigan WH. All-optical recording and stimulation of retinal neurons in vivo in retinal degeneration mice. *PLoS ONE*. 2018;13:e0194947.
125. Miller EB, Zhang P, Ching K, Pugh EN Jr., Burns ME. In vivo imaging reveals transient microglia recruitment and functional recovery of photoreceptor signaling after injury. *Proc Natl Acad Sci USA*. 2019;116:16603–12.
126. Debarre D, Botcherby EJ, Watanabe T, Srinivas S, Booth MJ, Wilson T. Image-based adaptive optics for two-photon microscopy. *Opt Lett*. 2009;34:2495–7.
127. Jesacher A, Thayil A, Grieve K, Debarre D, Watanabe T, Wilson T, et al. Adaptive harmonic generation microscopy of mammalian embryos. *Opt Lett*. 2009;34:3154–6.
128. Leroux CE, Grichine A, Wang I, Delon A. Correction of cell-induced optical aberrations in a fluorescence fluctuation microscope. *Opt Lett*. 2013;38:2401–3.
129. Liu YZ, Shemonski ND, Adie SG, Ahmad A, Bower AJ, Carney PS, et al. Computed optical interferometric tomography for high-speed volumetric cellular imaging. *Biomed Opt Express*. 2014;5:2988–3000.
130. Wells-Gray EM ZR, Finn SC, Greiner C, Werner JS, Choi SS, et al. Performance of a combined optical coherence tomography and scanning laser ophthalmoscope with adaptive optics for human retinal imaging applications. In: *Progress in Biomedical Optics and Imaging - Proceedings of SPIE*. Proceedings of SPIE. 2015;9335.
131. Cunefare D, Hickenpahler AL, Patterson EJ, Dubra A, Carroll J, Farsiu S. RAC-CNN: multimodal deep learning based automatic detection and classification of rod and cone photoreceptors in adaptive optics scanning light ophthalmoscope images. *Biomed Opt Express*. 2019;10:3815–32.
132. Ju MJ, Heisler M, Wahl D, Jian Y, Sarunic MV. Multiscale sensorless adaptive optics OCT angiography system for in vivo human retinal imaging. *J Biomed Opt*. 2017;22:1–10.
133. Jian Y, Lee S, Ju MJ, Heisler M, Ding W, Zawadzki RJ, et al. Lens-based wavefront sensorless adaptive optics swept source OCT. *Sci Rep*. 2016;6:27620.
134. Yang Q, Zhang J, Nozato K, Saito K, Williams DR, Roorda A, et al. Closed-loop optical stabilization and digital image registration in adaptive optics scanning light ophthalmoscopy. *Biomed Opt Express*. 2014;5:3174–91.
135. Park JH, Kong L, Zhou Y, Cui M. Large-field-of-view imaging by multi-pupil adaptive optics. *Nat Methods*. 2017;14:581–3.
136. Zhao Q, Shi X, Zhu X, Zheng Y, Wu C, Tang H, et al. Large field of view correction by using conjugate adaptive optics with multiple guide stars. *J Biophotonics*. 2019;12:e201800225.
137. Camino A, Ng R, Huang J, Guo Y, Ni S, Jia Y, et al. Depth-resolved optimization of a real-time sensorless adaptive optics optical coherence tomography. *Opt Lett*. 2020;45:2612–5.
138. Marcos S, Werner JS, Burns SA, Merigan WH, Artal P, Atchison DA, et al. Vision science and adaptive optics, the state of the field. *Vis Res*. 2017;132:3–33.
139. Camino A, Pengxiao Z, Athwal A, Ni S, Jia Y, Huang D, et al. Sensorless adaptive-optics optical coherence tomographic angiography. *Biomed Opt Express*. 2020;11:3952–67.
140. Jung H, Liu J, Liu T, George A, Smelkinson MG, Cohen S, et al. Longitudinal adaptive optics fluorescence microscopy reveals cellular mosaicism in patients. *JCI Insight*. 2019;4:1–17.
141. Song H, Rossi EA, Latchney L, Bessette A, Stone E, Hunter JJ, et al. Cone and rod loss in Stargardt disease revealed by adaptive optics scanning light ophthalmoscopy. *JAMA Ophthalmol*. 2015;133:1198–203.
142. Nakatake S, Murakami Y, Funatsu J, Koyanagi Y, Akiyama M, Momozawa Y, et al. Early detection of cone photoreceptor cell loss in retinitis pigmentosa using adaptive optics scanning laser ophthalmoscopy. *Graefes Arch Clin Exp Ophthalmol*. 2019;257:1169–81.
143. Song H, Rossi EA, Stone E, Latchney L, Williams D, Dubra A, et al. Phenotypic diversity in autosomal-dominant cone-rod dystrophy elucidated by adaptive optics retinal imaging. *Br J Ophthalmol*. 2018;102:136–41.
144. Nakanishi A, Ueno S, Hayashi T, Katagiri S, Ito Y, Kominami T, et al. Changes of cone photoreceptor mosaic in autosomal recessive bestrophinopathy. *Retina*. 2020;40:181–6.
145. Battu R, Akkali MC, Bhanushali D, Srinivasan P, Shetty R, Berendschot TT, et al. Adaptive optics imaging of the outer retinal tubules in Bietti's crystalline dystrophy. *Eye (Lond)*. 2016;30:705–12.
146. Gocho K, Akeo K, Itoh N, Kameya S, Hayashi T, Katagiri S, et al. High-resolution adaptive optics retinal image analysis at early stage central areolar choroidal dystrophy with prph2 mutation. *ophthalmic surg lasers imaging. Retina*. 2016;47:1115–26.
147. Ra E, Ito Y, Kawano K, Iwase T, Kaneko H, Ueno S, et al. Regeneration of photoreceptor outer segments after scleral buckling surgery for rhegmatogenous retinal detachment. *Am J Ophthalmol*. 2017;177:17–26.
148. Yokota S, Ooto S, Hangai M, Takayama K, Ueda-Arakawa N, Yoshihara Y, et al. Objective assessment of foveal cone loss ratio in surgically closed macular holes using adaptive optics scanning laser ophthalmoscopy. *PLoS ONE*. 2013;8:e63786.
149. Debellemanniere G, Flores M, Tumahai P, Meillat M, Bidaut Garnier M, Delbosc B, et al. Assessment of parafoveal cone density in patients taking hydroxychloroquine in the absence of clinically documented retinal toxicity. *Acta Ophthalmol*. 2015;93:e534–40.

150. Agarwal A, Soliman MK, Hanout M, Sadiq MA, Sarwar S, Jack LS, et al. Adaptive optics imaging of retinal photoreceptors overlying lesions in white dot syndrome and its functional correlation. *Am J Ophthalmol*. 2015;160:806–16.e2.
151. Nakamura T, Hayashi A, Oiwake T. Recovery of macular cone photoreceptors in Vogt-Koyanagi-Harada disease. *Graefes Arch Clin Exp Ophthalmol*. 2018;256:387–94.
152. Lammer J, Prager SG, Cheney MC, Ahmed A, Radwan SH, Burns SA, et al. Cone photoreceptor irregularity on adaptive optics scanning laser ophthalmoscopy correlates with severity of diabetic retinopathy and macular edema. *Invest Ophthalmol Vis Sci*. 2016;57:6624–32.
153. Razeen MM, Cooper RF, Langlo CS, Goldberg MR, Wilk MA, Han DP, et al. Correlating photoreceptor mosaic structure to clinical findings in stargardt disease. *Transl Vis Sci Technol*. 2016;5:6.
154. Lin R, Shen M, Pan D, Xu SZ, Shen RJ, Shao Y, et al. Relationship between cone loss and microvasculature change in retinitis pigmentosa. *Invest Ophthalmol Vis Sci*. 2019;60:4520–31.